

Surface plasmons regulate photon absorbance, photo response and carrier injection in Ga_2O_3 photodetectors

Zhi-Kang Song(宋志康), Xiang-Xi Meng(孟祥熙), Pu-Yang Gao(高溥阳), Jia-Han Zhang(张嘉汉), and Zeng Liu(刘增)

Citation: Chin. Phys. B, 2026, 35 (**8**): 088501. DOI: 10.1088/1674-1056/ae5f07
http://cpb.iphy.ac.cn; http://iopscience.iop.org/cpb

What follows is a list of articles you may be interested in

Self-powered horizontally structured n-n heterojunction photodetector based on Si-GaN/β-Ga_2O_3 for UV detection

Muzi Li(李木子), Maolin Zhang(张茂林), Xueqiang Ji(季学强), Shan Li(李山), Lili Yang(杨莉莉), and Weihua Tang(唐为华)

Chin. Phys. B, 2026, 35 (**2**): 028502. DOI: 10.1088/1674-1056/adee8d

Unraveling the role of dangling bonds passivation in amorphous Ga_2O_3 for high-performance solar-blind UV detection

Zhengru Li(李正濡), Rui Zhu(朱锐), Huili Liang(梁会力), Shichen Su(宿世臣), and Zengxia Mei(梅增霞)

Chin. Phys. B, 2025, 34 (**7**): 078502. DOI: 10.1088/1674-1056/adcb24

β-Ga_2O_3 junction barrier Schottky diode with NiO p-well floating field rings

Qiming He(何启鸣), Weibing Hao(郝伟兵), Qiuyan Li(李秋艳), Zhao Han(韩照), Song He(贺松),Qi Liu(刘琦), Xuanze Zhou(周选择), Guangwei Xu(徐光伟), and Shibing Long(龙世兵)

Chin. Phys. B, 2023, 32 (**12**): 128507. DOI: 10.1088/1674-1056/accf69

The growth and expansive applications of amorphous Ga_2O_3

Zhao-Ying Xi(奚昭颖), Li-Li Yang(杨莉莉), Lin-Cong Shu(舒林聪), Mao-Lin Zhang(张茂林), Shan Li(李山), Li Shi(史丽), Zeng Liu(刘增), Yu-Feng Guo(郭宇锋), and Wei-Hua Tang(唐为华)

Chin. Phys. B, 2023, 32 (**8**): 088502. DOI: 10.1088/1674-1056/accf81

One ε-Ga_2O_3-based solar-blind Schottky photodetector emphasizing high photocurrent gain and photocurrent-intensity linearity

Yue-Hua An(安跃华), Zhen-Sen Gao(高震森), Yu Guo(郭雨), Shao-Hui Zhang(张少辉), Zeng Liu(刘增), and Wei-Hua Tang(唐为华)

Chin. Phys. B, 2023, 32 (**5**): 058502. DOI: 10.1088/1674-1056/acb75b

---

REVIEW

Surface plasmons regulate photon absorbance, photo response and carrier injection in Ga_2O_3 photodetectors

Zhi-Kang Song(宋志康), Xiang-Xi Meng(孟祥熙), Pu-Yang Gao(高溥阳), Jia-Han Zhang(张嘉汉)†, and Zeng Liu(刘增)‡

School of Electronic Information Engineering, Electronic-Photonic Smart Sensing Device R&D Team, Inner Mongolia Key Laboratory of Intelligent Communication and Sensing and Signal Processing, Inner Mongolia University, Hohhot 010021, *China*

(Received 18 March 2026; revised manuscript received 2 April 2026; accepted manuscript online 14 April 2026)

Ultrawide bandgap semiconductor gallium oxide (Ga_2O_3), with a natural bandgap of approximately 4.9 eV, has been extensively utilized in constructing solar-blind deep ultraviolet (DUV) photodetectors. To address the persistent challenges of high dark current and low photoresponsivity, metal nanostructured surface plasmons have been introduced to generate localized electric fields, thereby enhancing photodetection performance. Incident photons excite hot electrons within the metallic structures, which are subsequently injected into the photoactive semiconductor layer. When the resonance peak of the plasmonic structure matches the absorption peak of Ga_2O_3 layer, localized surface plasmon resonance (LSPR) significantly boosts photon absorption and responsivity. Concurrently, the localized interfacial barrier restricts carrier transport, effectively suppressing dark current. This enhancement stems from charge density oscillations within the metallic nanoparticles, facilitating strong plasmon–exciton coupling. In this review, we systematically discuss Ga_2O_3-based solar-blind DUV photodetectors decorated with metal nanostructures, covering photoconductive, array, and heterojunction architectures. Furthermore, advances in broadband detection mechanisms, complex plasmonic designs, and subwavelength optics are explored. Compared with conventional devices, plasmon-enhanced photodetectors typically exhibit responsivity improvements from $\sim$ 0.1 A/W to over tens of A/W and reduced dark current by 1–2 orders of magnitude. Finally, current challenges and future perspectives are outlined. However, challenges such as poor controllability of nanoparticle distribution, stability issues, and the trade-off between enhanced responsivity and increased noise remain to be addressed.

Keywords: gallium oxide, surface plasmon, local field enhancement, solar-blind photodetection

PACS: 85.60.Gz

DOI: 10.1088/1674-1056/ae5f07 **CSTR:** 32038.14.CPB.ae5f07

1. Introduction

Semiconductors have been the footstone for developing electronic and optoelectronic devices, since Faraday discovered the effect of temperature on the resistance of AgS in 1833. Moreover, transistors invented at Bell Labs in 1947 opened an era in which semiconducting materials came to the microelectronic stage.[1] Modern electronics and optoelectronics strongly depend on the development of semiconductors and related techniques. Ultraviolet (UV) photodetectors, as one kind of optoelectronic device, are essential components in the modern solid-state optoelectronic industry.[2–6] In Fig. 1(a), UV rays, as the sensing target, are divided into UV-A (315–400 nm), UV-B (280–315 nm), UV-C (200–280 nm), and VUV (10–200 nm) wavebands.[7,8] The photodetection wavebands of the used semiconductor materials have a direct correlation with their optical bandgap (E_g). For research on UV photodetectors, wide bandgap semiconductors with E_g of over 3 eV are required.[9,10] Currently, ZnO,[11–13] SiC,[14–16] and GaN[17–19] are commonly used in fabricating UV-A and UV-B photodetectors. Diamond,[20] perovskite PEA_2PbBr_4,[21] and AlN[22] are suitable candidates for performing VUV photodetection. Additionally, UV-C, also called solar-blind deep UV, rarely appears at the Earth's surface due to the protection of the ozone layer. Thus, solar-blind deep UV photodetection features high sensitivity and low interference noise,[23,24] suggesting huge potential in the fields of environmental monitoring, health care, fire alarm, and optical communications.[25] To achieve this purpose, AlGaN[26–29] and MgZnO[30,31] multicomponent alloys were developed for performing solar-blind UV photodetection. However, by current science and technology, they are limited by high growth temperatures and poor controllability of the crystal structure, respectively.[32] A rising star material, gallium oxide (Ga_2O_3), has come to the center stage, catering for developing high-power electronics and solar-blind UV optoelectronics.[33–37] This is owing to the promising material properties, such as a high Baliga's figure of merit (BFoM) of over 3400, a large E_g of $\sim$ 4.9 eV, and a light absorbance cut-off wavelength of below 280 nm.[38] These suitable parameters make Ga_2O_3 a promising candidate for

†Corresponding author. E-mail: jiahan_zhang@outlook.com

‡Corresponding author. E-mail: zengliu@imu.edu.cn

© 2026 Chinese Physical Society and IOP Publishing Ltd. All rights, including for text and data mining, AI training, and similar technologies, are reserved.

fabricating solar-blind deep UV photodetectors.[39] As shown in Fig. 1(b), operating as a photoconductor, Ga_2O_3-based metal–semiconductor–metal (MSM) Ohmic-type detectors are reported extensively. As early as 2007, Oshima *et al.* used molecular beam epitaxy (MBE) technology to grow a Ga_2O_3 thin film to fabricate a photoconductive detector.[40] It always exhibits high photoresponse but has a low response speed. Schottky-type metal–semiconductor (M-S) photodiodes are also constructed to improve the response speed and reduce operation noise owing to the M-S interfacial barrier (i.e., Schottky barrier).[41] Moreover, heterojunction photodetectors are introduced to feature the advantages of low noise, fast speed, broadband sensing, and avalanche. To date, the highest responsivity (R) of 7.08 A/W at zero bias was achieved in a Ga_2O_3/SnO_x heterojunction photodetector,[42] highlighting an ultrahigh-performance self-powered photodetection. Promising progress has been achieved in performing solar-blind deep UV photodetection based on this new-generation ultra-wide-bandgap semiconductor Ga_2O_3.[39,43]

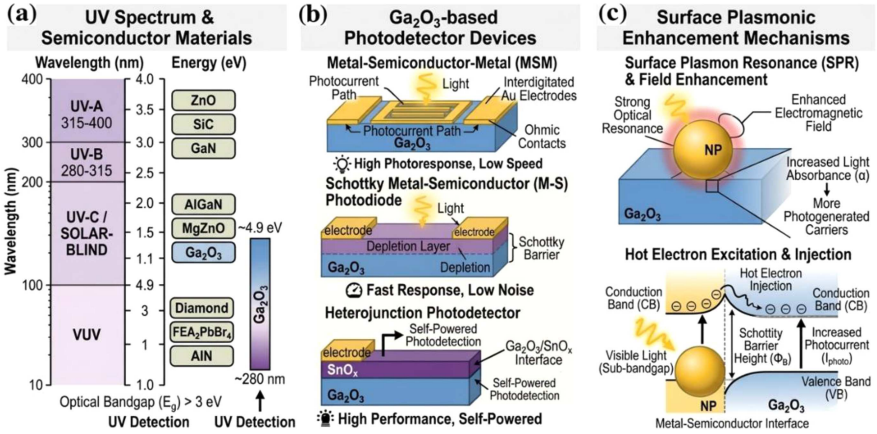


Fig. 1. (a) Comparison of UV spectral bands and wide bandgap semiconductors, highlighting the solar-blind advantages of Ga_2O_3. (b) Typical architectures of Ga_2O_3 photodetectors, including MSM, Schottky M-S, and heterojunction structures. (c) Schematic illustration of surface plasmonic enhancement mechanisms: (top) localized surface plasmon resonance (LSPR) induces strong electromagnetic field confinement near metal nanostructures, significantly enhancing light absorption in Ga_2O_3; (bottom) non-radiative plasmon decay generates energetic hot electrons, which overcome the Schottky barrier and inject into the semiconductor, contributing to photocurrent. Meanwhile, the formation of localized interfacial barriers can suppress carrier recombination and dark current, leading to improved signal-to-noise ratio.

In view of tuning photodetection performance, altering the structure of semiconductors could change the electromagnetic properties, which would lead to new concepts and novel phenomena[44] via drawing analogies between light and electrons.[45] Plasmonic metal nanoparticles show an opportunity for merging electronics and photonics at a nanoscale dimension,[46,47] which could enhance the electromagnetic field in the vicinity of a nanoscale metal surface. The integrated plasmonic nanoparticles with Ga_2O_3 would display strong optical resonance and hot electron excitation at the MS interface,[48] thus enhancing the photodetection behaviors by strong light absorption and effective carrier injection. This is owing to the stronger interaction between light and matter (i.e., light-Ga_2O_3 interaction for this review topic), based on the classical optoelectronic effect.[49] As shown in Fig. 1(c), the core mechanism of surface plasmon enhancement includes resonance and hot electron excitation, stemming from distinct optical absorption mechanisms in metal nanoparticles.[50–52]

The selection and integration of metal nanostructures (e.g., Al, Ag, and Au) play a crucial role in determining the performance of plasmon-enhanced photodetectors. The effectiveness of this enhancement is primarily governed by the localized surface plasmon resonance (LSPR), whose characteristic absorption wavelength is not only intrinsic to the metal type but also highly sensitive to geometric parameters such as size, shape, and interparticle spacing. Consequently, the resonance peak of these metals can be precisely modulated across a wide spectral range by optimizing growth techniques and deposition parameters. To maximize the performance of solar-blind photodetectors, it is essential to tailor the LSPR absorption peak of the selected metal to synergistically match the intrinsic absorption edge of Ga_2O_3. For instance, while Al is naturally suited for the DUV region, the plasmonic response of Ag or Au can also be blue-shifted toward the DUV range by reducing their dimensions or altering their morphology. Such spectral matching ensures optimal near-field coupling and efficient hot-carrier injection, which are fundamental to enhancing the responsivity and narrowing the spectral selectivity of the resulting devices. This serves as a pathway to achieve high optoelectronic gain.[53] In particular, photoconductive detectors have no gain intrinsically.[54] Leveraging the ultrahigh field enhancement and subwavelength field confinement, the Ga_2O_3-based plasmonic photodetectors are expected to be improved and applied in fields of photonic circuits,[55] biosensing,[56,57] surface-enhanced Raman scattering,[58] optical amplifiers,[59,60] etc.

In this review, the surface-plasmon-enhanced Ga_2O_3-based solar-blind deep-UV photodetectors are summarized

and discussed for developing new types of optoelectronic devices. Specifically, Ga_2O_3-based solar-blind deep-UV photodetectors decorated by metal nanostructures will be reviewed and discussed in detail, including photoconductive detectors, photodetector arrays and heterojunction photodetectors. Furthermore, based on the surface/interface modification by surface plasmons in Ga_2O_3-based photodetectors, the recent progress and inherent physical mechanism of broadband photodetection, complex plasmonic structure design, and subwavelength optics are also discussed.

2. Mechanism

Metal nanoparticles contribute to the local field along the M-S interfaces. Due to the natural light absorbance properties of metals and semiconductors, the surface plasmon polariton (SPP) contributes to a local field inside and/or outside the metal nanoparticles.[61,62] It is due to the oscillation of surface charge density (usually caused by external motivations) as shown in Fig. 2(a); electromagnetic wave modes are bound to the interface between a nanostructured metal and a semiconductor material.[63] As shown in Fig. 2(b), the excitation of LSPR by an incident light will lead to strong light scattering. This would cause an enhancement of the localized electromagnetic field and intense surface plasmon absorbance wavebands. Thus, the frequency (or absorbance wavelength) of the used metal nanoparticles and photoactive materials should be close to each other. Note that, the optical properties of metal nanoparticles seriously depend on the size, shape, distribution and environment.[64] In Fig. 2(c), LSPR does not happen, and certainly light scattering is avoided. Its electromagnetic field lines around the metal nanoparticle seem regular, and hardly change directions. Under such a condition, beyond the enhancement of the localized field, the excited hot electrons will inject into the material layer in a photodetector. For a LSPR enhanced photodetectors, the plasmon-induced resonance energy transfer (PIRET) and hot electron injection are concurrent.

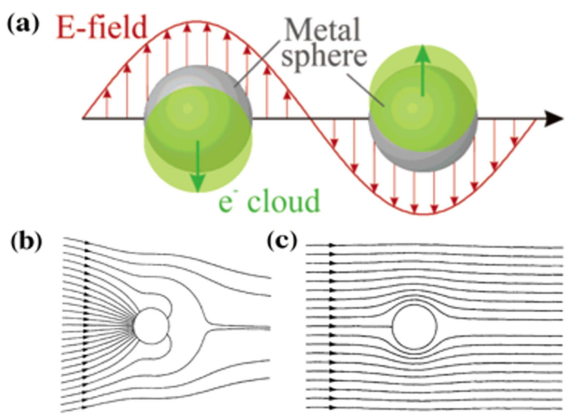


Fig. 2. (a) Schematic diagram of the plasmon oscillation for a metallic nanosphere, where a displacement of the electron cloud (e cloud) occured relative to the nuclei. Reproduced with permission from Ref. [64], Copyright 2003, American Chemical Society. Electric field lines of the Poynting vector around a small nanostructured metallic sphere when localized surface plasmon resonance (b) occurred and (c) did not happen, reproduced with permission from Ref. [65], Copyright 1998, Wiley-VCH Verlag GmbH & Co. KGaA.

2.1. Hot electron transfer

If the absorbance peaks of metal nanoparticles and active semiconductor layer are not next to each other closely, the LSPR would not effectively influence the photodetection. While, lots of free electrons in metal nanoparticles can be excited and injected to the semiconductor across the metal–semiconductor interface[52] as shown in Fig. 3, in a current loop of a photodetector. As a result, the output current signal can be also improved. This is owing to the hot electron transfer by fabricating nanoparticles on the surface of photosensitive semiconductors.[66] Worthy to be noted, the hot electron transfers also occurred in the LSPR enhanced photodetectors.

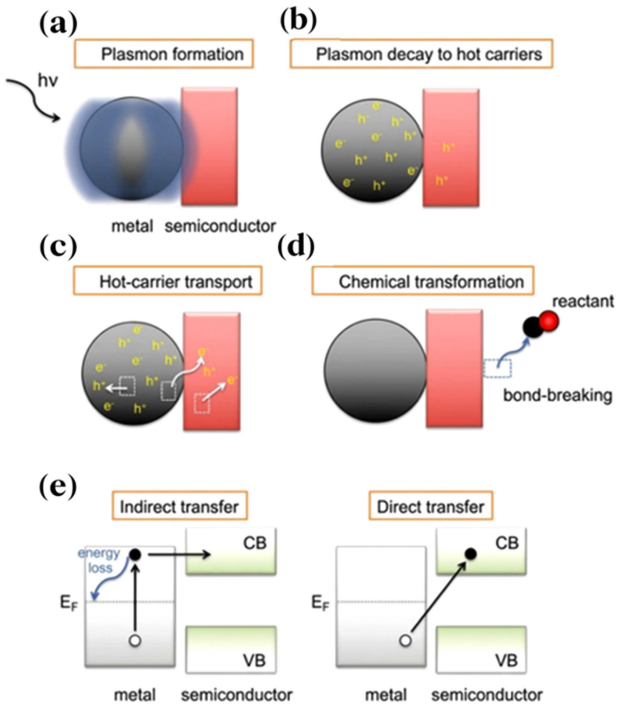


Fig. 3. Plasmonic hot electron engineering at metal–semiconductor interfaces. Processes schematics of (a) plasmon formation, (b) plasmon decay to hot carriers (for Ga_2O_3, the majority carrier is electron), (c) hot electrons transport in the main body structure of the photodetector, (d) chemical transformation, (e) indirect/direct transfer between metal and semiconductor. Reproduced with permission from Ref. [52], Copyright 2025, Wiley-VCH GmbH.

2.2. Local surface plasmon resonance

LSPR is a plasmon–exciton coupling strategy to enhance the photodetection performance of a photodetector. It is a spontaneous strong coupling[67,68] because the absorbance peaks of the metal nanoparticles and the active semiconductor layer should be very close, or even the same. In such a condition, the enhanced photodetection performance is attributed to both the local field confinement and plasmon–exciton coupling, as shown in Fig. 4. In fact, the resonance wavelength

depends on the size, shape, and local dielectric environment of nanoparticles.[50,69–74]

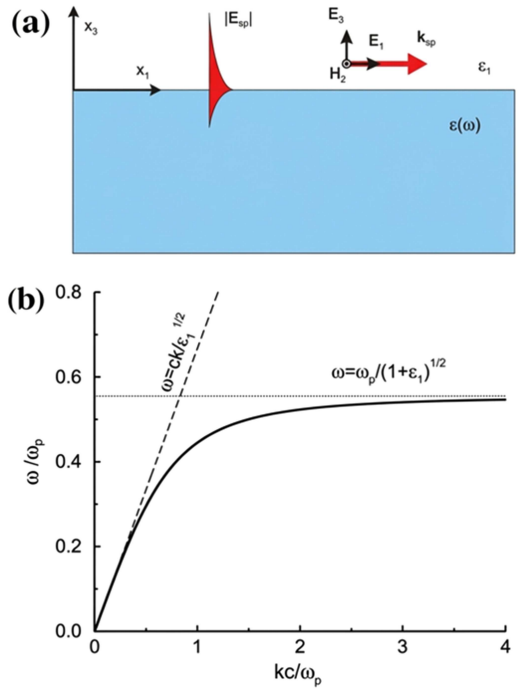


Fig. 4. (a) Surface plasmon polariton at metal–semiconductor interface, (b) dispersion of SPP at an interface of metal and semiconductor. Reproduced with permission from Ref. [63], Copyright 2005, Elsevier.

3. Progress on Ga_2O_3 plasmonic photodetectors

Based on the fundamental mechanisms discussed in Section 2, including hot electron transfer and LSPR, recent research efforts have focused on leveraging these effects to enhance the performance of Ga_2O_3-based photodetectors. In the following section, we summarize the latest progress in plasmon-enhanced Ga_2O_3 photodetectors, categorized by device architectures and dominant enhancement mechanisms, providing a comprehensive overview of their performance improvements and underlying physics.

As early in 2008, Hsieh *et al.*[75] reported a nanophotonic switch based on gold-in-Ga_2O_3 peapod nanowires, when the nano/micro structured metal decorates Ga_2O_3 to tune its optoelectronic performances began. In their report, along with uniform twinned Ga_2O_3 nanowires, the Au-in-Ga_2O_3 peapods could spontaneously crystallize via the reaction between Au, Ga, and silica at an annealing temperature of 800 °C. Irradiated by laser, an enhanced photoconductivity was observed owing to the LSPR effect of Au and Ga nanoparticles. During which, the electromagnetic field enhancement along the Au-metal/Ga_2O_3 interface contributes much. Its photocurrent (I_{photo}) reached 103.25 pA, indicating highly efficient photo response behaviours. Their co-workers[76] investigated the plasmon resonance spectroscopy of the gold-in-Ga_2O_3 peapod core–shell structured nanowires, where the light scattering peaks were suggested to result from the LSPR of Au nanostructures in the Ga_2O_3 nanowires. The resonance peaks showed a red-shift as the diameters of Au nanopeas increased. This core–shell nanostructure may induce a tunable local optical field via changing the sizes of metal nanoparticles, to extend the Mie theory.[61,77]

This review discusses the progress of surface plasmon enhanced Ga_2O_3-based solar-blind deep UV photodetectors. The enhancement is discussed based on hot electron transfer/injection and LSPR. The effects of LSPR on photodetection performance are carried forward from photoconductive, array, and heterojunction photodetectors. In this context, the metal nanostructure surface plasmons play a role in modifying the surface and interface.

3.1. Hot electron transfer and injection

Surface plasmon can be seen as a wave that can propagate along the surface of a metal (metal nanostructures in this review). It represented enormous progress in surface science pioneered in the 1950s.[78] The induced surface plasmons as waves can interact with the incident light, i.e., interaction between light and matter happens. Here, an opportunity comes to the semiconductor device community: the functionalities and performances of devices are expected to be adjusted with more freedom. When this surface technology is integrated into photodetection devices, hot carrier (electron for n-Ga_2O_3) transfer and injection across the metal–semiconductor interface become a vital subject, which may largely determine the device performance.

To view current development of Ga_2O_3-based photodetectors that are decorated by surface plasmons. In 2016, An *et al.*[79] achieved higher performance Ga_2O_3 solar-blind UV photodetector by Au surface plasmon effect. The Au thin film was deposited on the surface of β-Ga_2O_3 thin film and then became nanoparticles after post-annealing processing as shown in Fig. 5(a), since metal can always be heated to melt into a globular shape. This is a general pathway to prepare metal nanoparticles. The prepared Au NPs/β-Ga_2O_3 composite structure could effectively absorb light around 250 nm and 510 nm, as shown in Fig. 5(b). The longer wavelength light absorbance is owing to the integration of Au nanoparticles. And, as shown in Fig. 5(c), it exhibited higher photo responsivity (R) of 103 A/W at 254 nm and 532 nm light illuminations than that of 50 A/W at 254 nm light illumination only. However, R at 532 nm light illumination only was just 0.1 A/W, suggesting bad photosensitive property to 532 nm light. What can be concluded is that the photo response enhancement is due to the surface plasmon effect. In which, lots of free electrons in Au nanoparticles were motivated to be injected to the active Ga_2O_3 layer, and then tunnel to the counter electrodes. Besides, Al nanoparticles was also introduced to decorate metastable α-Ga_2O_3,[80] as shown in Fig. 5(d). As

shown in Fig. 5(e), the highest R of 3.36 A/W at 244 nm light illumination was achieved, where 25 μm finger spacing distance (it is not the main topic for this review, and related to the photoconductivity concerns). This Al nanoparticles decorated α-Ga_2O_3 photodetector displayed 244 nm/320 nm rejection ratio ($R_{244\ nm}/R_{320\ nm}$) of over 240 (i.e., ratio of R at 244 nm and 320 nm). Similarly, Al nanoparticles could enhance the photo response, akin to the Au nanoparticles. Essentially, this enhancement is due to the surface plasmon oscillation, that promoted a local field along the metal-Ga_2O_3 interface. As shown in Fig. 5(f), a surface energy level was located at the top of valence band, the surface states below these levels were empty. After the light is illuminated upon the device, the photogenerated electrons would fill the empty donor surface states, then the energy-band was even-up. When the Al NPs were involved in the device, a localized field resulted from Al nano plasmonic enhancement was achieved. Hence, more electrons will lead to a significant decrease in the surface potential, which results in a stronger energy band bending trend. As shown in Fig. 5(g), Shu *et al* fabricated Ag nanoparticles plasmonic In-doped Ga_2O_3 (InGaO) solar-blind UV photodetectors,[81] in which the small scaled Ag nanoparticles were employed. The introduction of Ag nanoparticles played a role of surface modification in enhancing photoabsorbance. As a result, by the decoration of Ag nanoparticles, the R increased to 193 mA/W, and the external quantum efficiency (EQE) had reached 100% at bias of −6 V. From its energy-band analysis in Fig. 5(h), Ag has relatively small work function, and contribute to low Schottky barrier height. Meanwhile, lots of free electrons in Ag metal would transport in the current loop of fabricated photodetector, then enhance the photo-response performance and photo-sensitivity. In this device, the plasmon–exciton coupling and hot electron transfer contributed synergistically to the improvement of photodetection. What is worthy to be noted, the Ag nanoparticles with small sizes could resonance with the Ga_2O_3. Since the optical properties of metal nanoparticles are seriously related to the size and shape.[64,69] In addition, the high dielectric MgO passivation layer[82] was furtherly inserted into the InGaO photodetector structure.[83] By enhancements of Ag plasmonic effect, optical properties of MgO and high-k surface passivation, the R of Ag NPs/MgO/InGaO photodetector displayed furtherly improved performances towards optical communication. The R was as high as 2.4 A/W, and EQE reached up to 1136%.

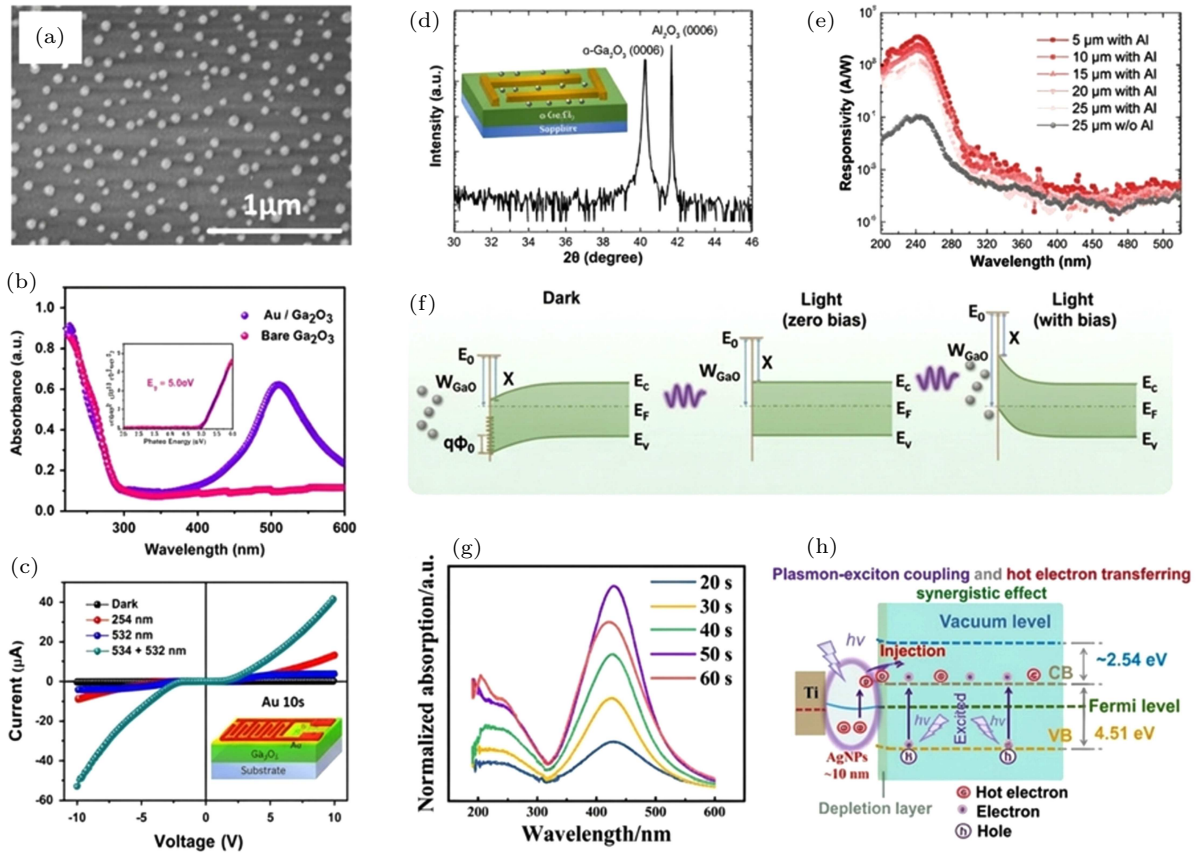


Fig. 5. (a) A scanning electron microscope of the Au nanoparticles in the surface of Ga_2O_3 thin film, (b) the UV-visible absorbance spectra with and without Au nanoparticles decoration, and (c) the Au decorated β-Ga_2O_3 current–voltage curves in the dark and under illuminations, produced with permission from Ref. [79], Copyright 2016, Elsevier. (d) Schematic and x-ray diffraction pattern of the Al nanoparticles decorated α-Ga_2O_3 thin film, (e) spectral response with different finger spacings, (f) detailed energy-band diagram, reproduced with permission from Ref. [80], Copyright 2019, American Chemical Society. (g) UV-visible absorbance spectra of the Ag nanoparticles decorated InGaO, where the growth time of Ag is different, (h) the schematic energy-band diagram and operating mechanism of the Ag nanoparticles on InGaO thin film, reproduced with permission from Ref. [81], Copyright 2024, American Chemical Society.

3.2. Local surface plasmon resonance

3.2.1. Photoconductive detectors

Confined to the metallic NPs, in such a situation that excitation of localized surface plasmons excited by the incident light with a certain wavelength displays a very close absorbance characteristic (absorbance peak) with photoactive materials.[68] LSPR results in strong light scattering, and the localized electromagnetic field around the metal NPs can be enhanced. The plasmons and excitons (electrons for n-Ga_2O_3) would show a strong coupling effect[67] to contribute to better photoresponse performances, especially for a photodetection device. Photoabsorbance is well enhanced via such a process. In other words, the light absorbance peak should match between the metal NPs and the photosensitive material layer. Importantly, the absorbance of the metallic NPs could be determined by the types, sizes, shapes, and distributions, etc. This can provide more freedom to tune the performances of photodetectors tuned by the LSPR.

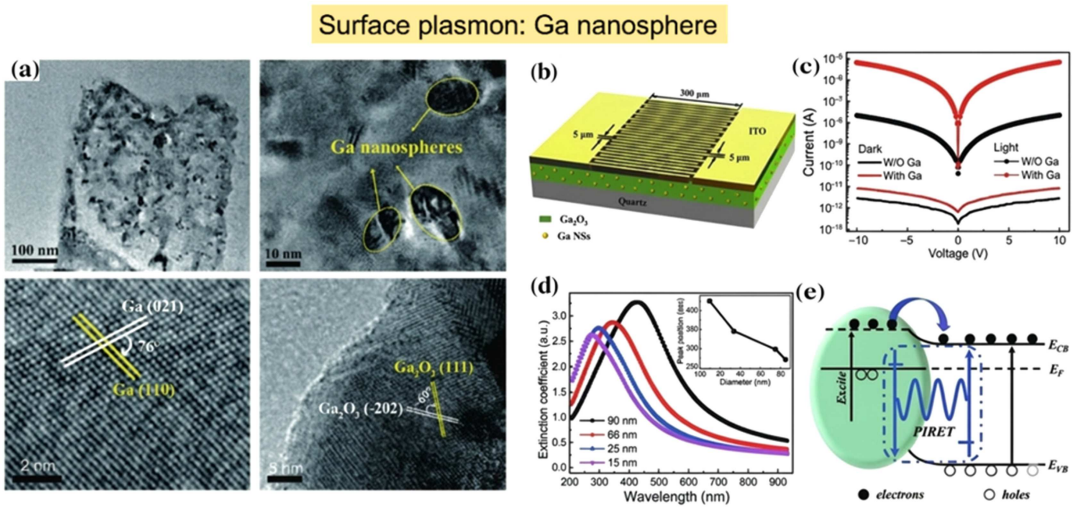


Fig. 6. Ga nanospheres surface plasmons enhanced Ga_2O_3-based photodetector: (a) transmission electron microscopy images of the Ga nanospheres decorated Ga_2O_3 thin film, (b) a schematic of the metal–semiconductor–metal photoconductive Ga/Ga_2O_3 nanocomposite photodetector, (c) the current–voltage curves of the fabricated photodetector in the dark and under illumination for those with and without Ga nanospheres, (d) the effect of diameters of Ga nanospheres on extinction spectra, (e) energy-band diagram of the Ga/Ga_2O_3 nanocomposite photodetector, reproduced with permission from Ref. [85], Copyright 2018, Science China Press and Springer-Verlag GmbH.

In 2018, Cui *et al.*[84] reported a solar-blind photodetector enhanced by Ga/Ga_2O_3 nanocomposite films. The Ga metal layer was pre-buried and the laminated Ga/Ga_2O_3 structure (with Ga nanosphere in it) was post-annealed. They found that the R and photocurrent (I_{photo}) first increased and then decreased as the thickness of the Ga layer increased. When the 20 nm Ga layer was used in this photodetector, the lowest I_{dark} of 8.52 pA (at 10 V), highest photo-to-dark current ratio (PDCR) of 8×10^5 and R of 2.85 A/W were achieved. Furthermore, the surface plasmon resonance effect was discussed in Ga nanospheres enhanced Ga_2O_3 photodetector. Ga nanospheres, which served as surface plasmons, were prepared on the surface of the Ga_2O_3 thin film.[85] As shown in Fig. 6(a), transmission electron microscopy (TEM) images of Ga/Ga_2O_3 nanocomposite films are displayed. They have different crystallization characteristics, and the diameters of these nanospheres range from 10 nm to 20 nm. This result indicates successful fabrication after the annealing process. This is also a common method to prepare metal nanostructures in plasmon-enhanced photodetectors.[86–89] The schematic diagram of the constructed photodetector is shown in Fig. 6(b). Its photo response performances are displayed in Fig. 6(c). Compared to the photodetector without Ga decoration, the I_{photo} increased from 2.23×10^{-8} A to 6.86×10^{-6} A. Meanwhile, the I_{dark} was also slightly improved. The increase of output currents both in the dark and under illumination is due to the strong coupling of surface plasmons. For the photodetectors with and without Ga nanosphere decoration, they exhibited stable and repeatable switching response and had no difference in response time. What can be concluded is that the introduction of Ga nanospheres does not influence the photogeneration and recombination processes. In Fig. 6(d), the extinction spectra of Ga nanospheres with different sizes are shown using spectroscopic ellipsometry tests. In fact, the sizes of the Ga nanospheres were controlled by changing the thicknesses of the Ga films. Obviously, the resonance peak displayed a blue shift as the diameter decreased, from the visible to the solar-blind UV region.[90] When the diameter of the Ga nanosphere was 15 nm, its surface plasmonic energy matched the energy band of Ga_2O_3 (generally stated as 4.9 eV). In this case, the photodetection enhancement for this device agrees well with the plasmon-induced resonance energy transfer (PIRET) mechanism[91] and direct electron transfer (DET).[92] Figure 6(e) is the schematic energy band diagram of the Ga surface plasmon enhanced Ga_2O_3 photodetector, which well illustrates the carrier transfer at the Ga/Ga_2O_3

interface. The free electrons on the surface of the Ga metal can oscillate in resonance with the incident UV light, thus serving as surface plasmons. The PIRET occurs from surface plasmons to Ga_2O_3 via a dipole–dipole interaction. Thus, the excitation of electrons in Ga_2O_3 is boosted, and the DUV response can be enhanced.

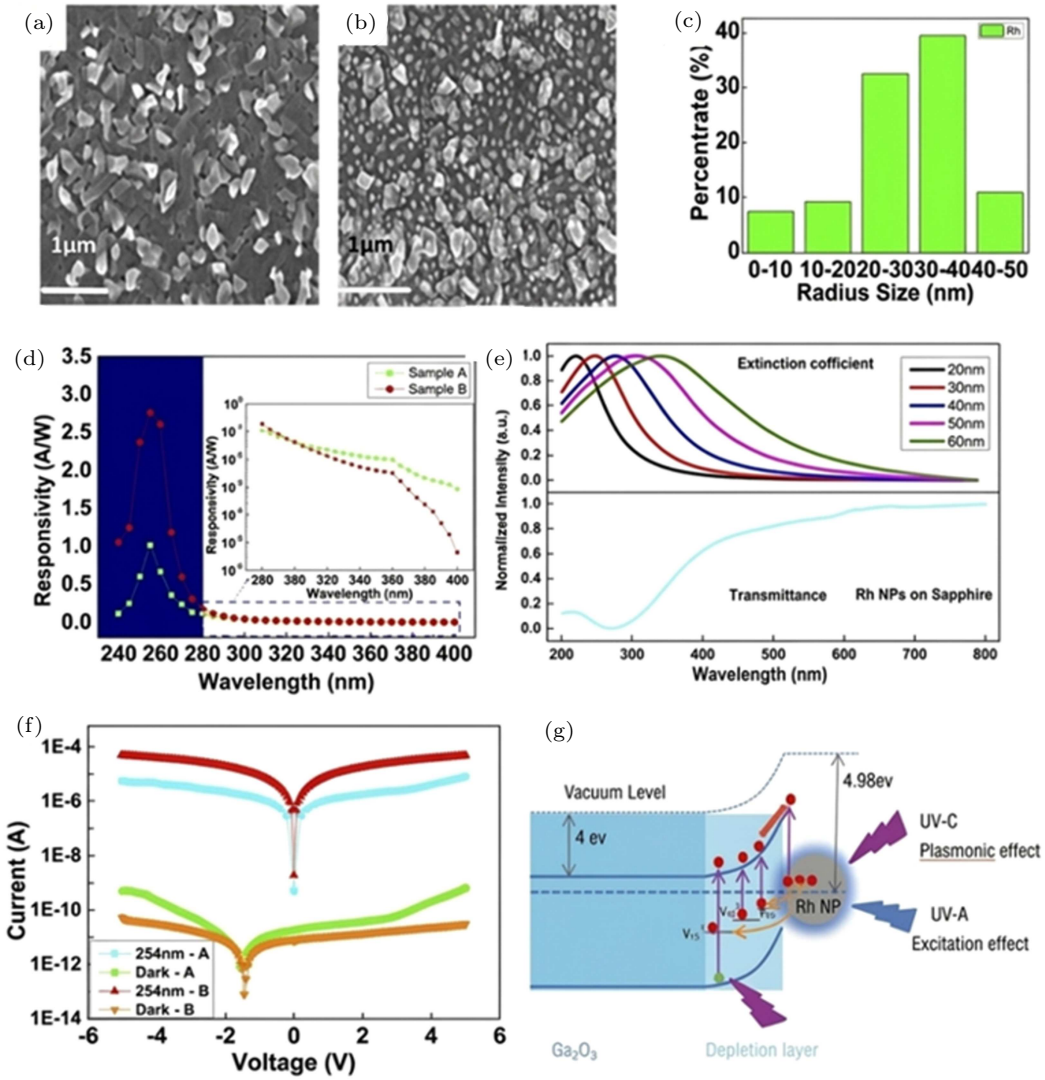


Fig. 7. Ru nanoparticles surface plasmons enhanced Ga_2O_3-based photodetector: high-resolution field emission scanning electron microscope images of Ga_2O_3 thin film (a) without and (b) with Ru nanoparticles, (c) the size distribution of Ru nanoparticles on the surface of Ga_2O_3 thin film, (d) the responsivity depending on the wavelengths at 5 V for both Ga_2O_3 photodetectors with and without nanoparticles, (e) the transmission spectra of the Ru nanoparticles on sapphire substrate with different radii by FDTD simulation and experiment, (f) current–voltage curves of Ga_2O_3 photodetectors with and without Ru nanoparticles in the dark and under illuminations, (g) schematic of Ga_2O_3 photodetectors with Ru nanoparticles, reproduced with permission from Ref. [95], Copyright 2020, Optical Society of America.

In addition to enhancing the photo response of a photodetector, reducing I_{dark} is also a key issue to improve the photo sensitivity. This matter is always realized in Schottky photodiodes[93] and heterojunction photodetectors,[94] which contain an interfacial barrier in them to restrain carriers. In photoconductive detectors, comparatively speaking, it is hard to achieve low I_{dark}. Concerning the discussed topic in this review, LSPR was used to form a localized Schottky barrier between metal nanoparticles and Ga_2O_3 semiconductor. The localized electric field strength was enhanced. As shown in Figs. 7(a) and 6(b), the field-emission SEM (FE-SEM) images of the Ga_2O_3 thin film with and without Ru nanoparticles are displayed.[95] The nanoparticle density was about 1.8×10^9 cm^{-2}, and its statistical summary is shown in Fig. 7(c). Whether Ru nanoparticles decorated Ga_2O_3 thin film or not, the spectral response peaks were located at 255 nm as shown in Fig. 7(d). While the R was improved from 1.01 A/W to 2.76 A/W after Ru nanoparticle decoration at wavelengths shorter than 300 nm, owing to the plasmonic effect of Ru nanoparticles. However, as shown in Fig. 7(d) inset, the R at wavelength becomes lower with Ru nanoparticles, translating to a higher light rejection ratio and excellent wavelength selectivity. To investigate the resonance wavelength,[96] the simulated extinction spectra of Ru nanoparticles with different sizes were performed by the finite difference time-domain (FDTD) method, as shown in Fig. 7(e). The peak

showed a blue shift as the diameter of the Ru nanoparticle decreased. The diameters between 20 nm and 40 nm could contribute to a plasmon resonance peak located at 220–280 nm. It is deduced that the plasmonic energy of prepared Ru nanoparticles matched the energy-band of Ga_2O_3. PIRET facilitates the excitation of electrons in Ga_2O_3, promoting the enhanced absorbance and the improved photo response. Moreover, the transmittance spectrum of Ru nanoparticles is also shown in Fig. 7(e), further illustrating that the enhanced performance is owing to the plasmonic effect of embedded Ru nanoparticles. As a result, the current–voltage curves are shown in Fig. 7(f). The Ru nanoparticles surface plasmon embedded Ga_2O_3-based photodetector displayed higher I_{photo} and lower I_{dark}. In addition to the aforementioned discussion on improved photo response (higher I_{photo}), low I_{dark} was achieved due to the development of an interfacial barrier at the Ru/Ga_2O_3 interface as shown in Fig. 7(g). The difference between the work function of Ru ($\sim$4.98 eV)[97] and the electron affinity of Ga_2O_3 ($\sim$4.00 eV)[98] leads to a localized Schottky barrier, thus localized depletion occurred on the surface of Ga_2O_3 near the Ru nanoparticles.[99]

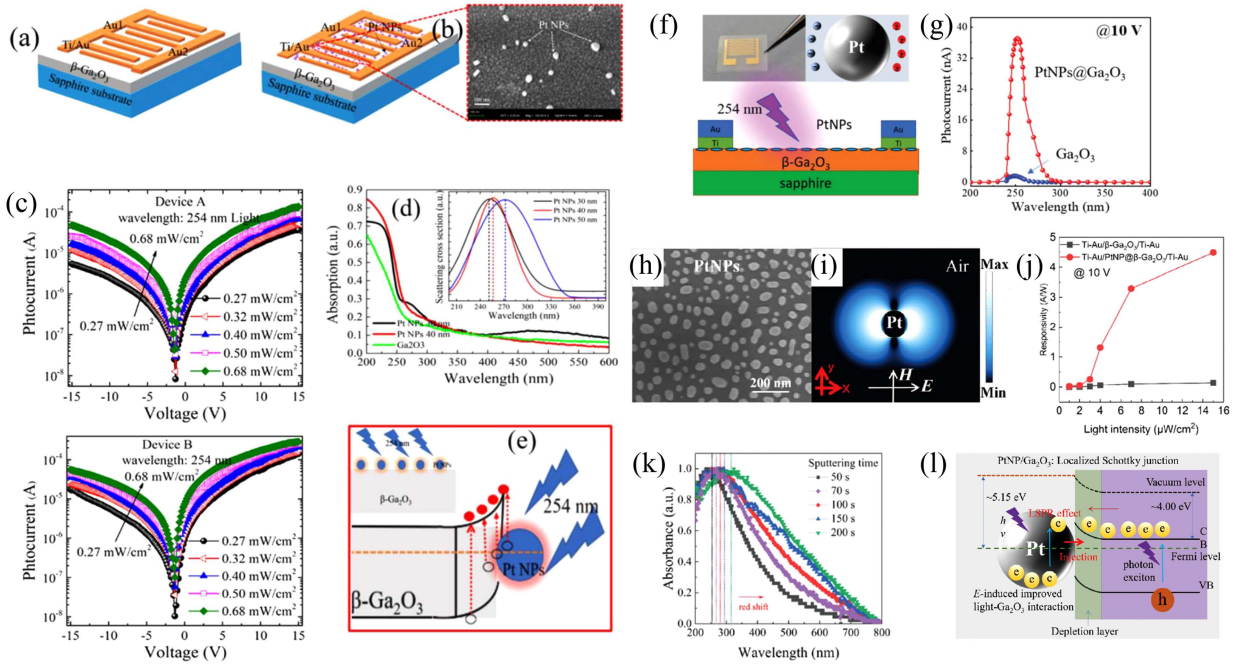


Fig. 8. Pt nanoparticles surface plasmons enhanced Ga_2O_3-based photodetector: (a) schematic diagrams of Ga_2O_3-based photodetectors (a) without and (b) with Pt nanoparticles, (c) the current–voltage curves under illuminations with different light intensities, (d) the UV-visible absorbance spectra of Ga_2O_3-based photodetectors with and without Pt nanoparticles, (e) energy-band diagram of Ga_2O_3-based photodetector with Pt nanoparticles, reproduced with permission from Ref. [100], Copyright 2021, Elsevier. (f) Schematic diagram of Pt nanoparticles decorated Ga_2O_3-based photodetector, (g) the spectral response of Ga_2O_3-based photodetectors with and without Pt nanoparticles, (h) the scanning electron microscopy image of Pt nanoparticles, (i) the top-view at x–y plane of the localized electric field, (k) the absorbance spectra of Pt nanoparticles on quartz grown for different times, (l) detailed schematic diagram of Ga_2O_3-based photodetector decorated by Pt nanoparticles, reproduced with permission from Ref. [101], Copyright 2023, IEEE.

Besides, Pt nanoparticles were also introduced into Ga_2O_3-based photodetectors to overcome the disadvantage of high I_{dark}.[100] As shown in Fig. 8(a), the schematic of the Ga_2O_3-based metal–semiconductor–metal-structured photodetector, and the Pt-nanoparticle-decorated one and the SEM image of Pt nanoparticles are shown in Fig. 8(b). The diameter of the Pt nanoparticles was around 40–45 nm. The I–V curves under illuminations (with different light intensities) for the Ga_2O_3 photodetector (device A) and Pt-decorated Ga_2O_3 photodetector (device B) are shown in Fig. 8(c). The I_{photo} increased with increasing light intensity, and device B had a higher I_{photo}. Figure 8(d) shows the absorbance spectra of the Ga_2O_3 photodetector with and without Pt nanoparticle decoration. The enhancement of light absorbance at DUV wavebands was realized by introducing Pt nanoparticles. As analysed in Fig. 8(e), under 254 nm light illumination, the incident light, acting as an electromagnetic wave, was coupled to the Pt nanoparticles, improving the light absorbance. Furthermore, Liu *et al*[101] fabricated a Ga_2O_3-based photodetector synergistically enhanced by high photon absorbance and carrier injection. Its schematic diagram is shown in Fig. 8(f). Its spectral response is displayed in Fig. 8(g), indicating higher photon absorbance for the Pt-nanoparticle-decorated Ga_2O_3-based photodetector. Figure 8(h) shows the SEM image of Pt nanoparticles (grown for 50 s) with clear morphology and distinct boundaries. Figure 8(i) is the top-view of the x–y plane of the developed localized electric field, displaying a symmetric dipole-plasmon mapping. The R increased as the light intensity increased, as shown in Fig. 8(j). The R of the Pt-decorated Ga_2O_3 photodetector was much higher than that of the Ga_2O_3

photodetector without Pt nanoparticle decoration. At a bias of 10 V, the R increased from 0.13 A/W to 4.49 A/W by virtue of the Pt nanoparticles. In Fig. 8(k), the absorbance spectra of Pt nanoparticles with different sizes (due to different sputtering times) are given. The absorbance peak showed a red shift as the sputtering time increased. As shown in Fig. 8(l), the localized electric field can be developed due to the redistribution of charges on the surface of the Pt nanoparticles, and meanwhile LSPR is produced. What's more, the incident light motivates free electrons in the Pt nanoparticles, and they then inject into the Ga_2O_3 layer.

The suppression of I_{dark} in plasmon-enhanced photodetectors can be attributed to the formation of localized Schottky barriers at the metal nanoparticle/Ga_2O_3 interface. Due to the difference in work function between the metal and semiconductor, band bending occurs near the interface, leading to the formation of depletion regions. These localized barriers act as potential obstacles that hinder the transport of thermally generated carriers under dark conditions. As a result, carrier injection is effectively suppressed unless sufficient photoexcitation is provided. Moreover, the spatially distributed nature of these nanoscale Schottky barriers further enhances carrier filtering, reducing leakage pathways and improving the signal-to-noise ratio. This mechanism is particularly important in photoconductive devices where intrinsic dark current is typically high.

3.2.2. Photodetector array

In this section, the effects of metal surface plasmons on the photodetection performance of Ga_2O_3-based photodetector array are discussed. Compared to the content in Subsection 3.2.1, the difference is that a more uniform distribution of nanoparticles is needed to guarantee the photodetection performance uniformity.

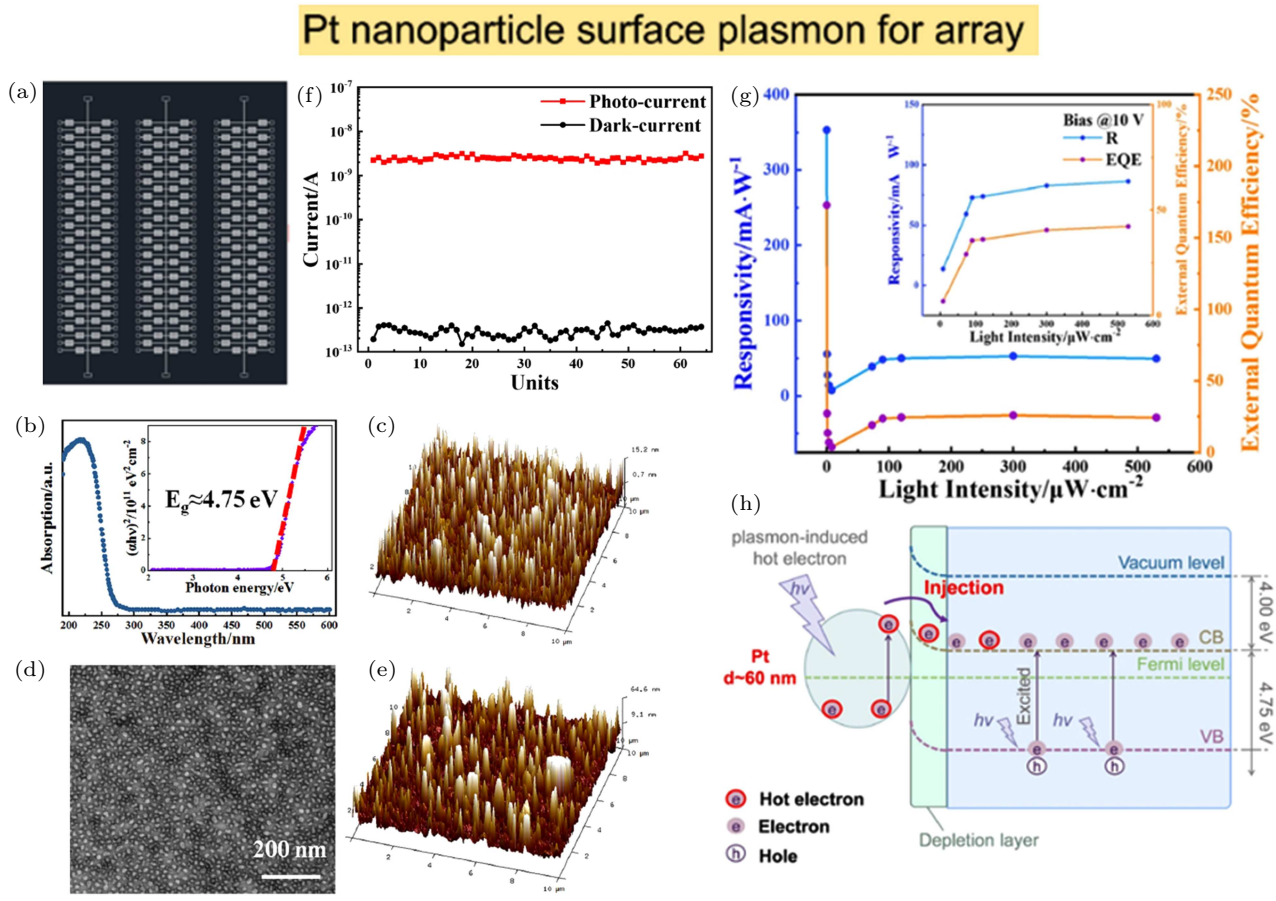


Fig. 9. Pt nanoparticles surface plasmons enhanced Ga_2O_3-based photodetector array: (a) schematic of the 16×4 linear photodetector array, (b) UV-visible absorbance spectrum and (c) AFM image of In-doped Ga_2O_3 thin film, (d) SEM image and (e) AFM image of the Pt nanoparticles on the sapphire substrate, (f) the dark current and photocurrent for all the units in array, (g) the light independent responsivity and external quantum efficiency, (h) schematic energy-band diagram of the Pt nanoparticles decorated In-doped Ga_2O_3 photodetector array, reproduced with permission from Ref. [102], Copyright 2024, Science China Press.

As shown in Fig. 9, Shu *et al.*[102] fabricated a 16×4 linear array solar-blind UV photodetector based on an InGaO thin film grown by plasma-enhanced chemical vapor deposition (PECVD). The photodetector array could provide more pixels in optical communications and imaging applications.[103–105] Figure 9(a) is the schematic diagram of the fabricated linear array based on the InGaO thin film. This array type features high frame rate and is often used in scenarios where high-speed detection is required, such as industrial inspection and medical imaging, where rapid imaging is needed. In Fig. 9(b), the ab-

sorbance spectrum of the InGaO thin film is shown and the optical bandgap of 4.75 eV was obtained, certifying the feasibility of solar-blind UV photodetection. Figure 9(c) shows the AFM image of the InGaO thin film, and the root mean square roughness of 5.24 nm provided a material foundation for constructing large-area photodetector arrays. Uniform photodetector performances are desired to increase the geometric accuracy when recording data in every unit in the array. Figures 9(d) and 9(e) are the SEM and AFM images of the Pt nanoparticles on a sapphire substrate. The size of Pt nanoparticles is tens of nanometres, showing a high degree of regularity. This is also a key factor in determining the uniform performances of the surface plasmon-enhanced photodetectors. As a result, the high-quality InGaO thin film contributed to high-performance photodetection. Especially, as shown in Fig. 9(f), the I_{dark} and I_{photo} in this photodetector array remain almost unchanged, displaying uniform photodetection performances. In addition, in Fig. 9(g), the light-intensity-dependent R and external quantum efficiency (EQE) are shown. They decrease as the light intensity increases at low light intensities. At high light intensities, the R and EQE did not change much. When the incident low-intensity light was illuminated upon the surface of the photodetector, relatively low photogenerated carriers and a short diffusion distance cause electron–hole recombination. Therefore, a low R was obtained in this photodetector under low-intensity light illumination. Moreover, LSPR did not effectively enhance the photodetection of this detector. As the light intensity increases, more photons result in highly excited hot electrons by plasmons. The photodetection performances were further improved owing to the highly effective carrier injection, as shown in Fig. 9(h). This study of the photodetector array explores its applications in optical imaging and water quality monitoring.

3.2.3. Heterojunction photodetector

Interface always plays serious role in device performance,[106–108] and the energy-band re-arrangement after heterojunction construction provides more freedoms to tune the device parameters.[4] Form the current development of Ga_2O_3-based solar-blind UV photodetectors, the Ga_2O_3-based heterojunction exhibited many advantages, such as low I_{dark}, high gain and fast response speed, etc. Thus, in this part, the effects of surface plasmons on the Ga_2O_3-based heterojunction photodetectors would be discussed in detail.

As shown in Fig. 10(a) inset, after the Ga_2O_3/NiO heterojunction fabrication, and the Pt nanoparticles were used to decorate the surface of upper Ga_2O_3 thin film.[109] The photodetection was enhanced by the surface plasmons and the interfacial barrier. Figure 10(a) is the SEM image of the Pt nanoparticles decorated Ga_2O_3, which was grown by magnetron sputtering. In comparison, as shown in Fig. 10(b), the current–voltage curves of Ga_2O_3/NiO heterojunction photodetector with and without Pt nanoparticles decoration are provided, in the dark and under illuminations. In which, the 254 nm deep UV light was used as light source. It displayed a rectification like a Schottky diode, as Ti and Ni were employed as asymmetrical electrodes. Ti/Ga_2O_3 and Ni/NiO metal–semiconductor exhibited nearly Ohmic contact, the rectifying characteristic was owing to the constructed interface of Ga_2O_3/NiO heterojunction. Importantly, the I_{dark} was obviously supressed, and I_{photo} was also slightly improved. This is beneficial from the introduction of Pt nanoparticles on the surface of Ga_2O_3 thin film. When the Ga_2O_3/NiO heterojunction worked as a photodetection device, the Pt nanoparticles enhance the optoelectronic performances. I_{photo} was enhanced at both forward and reverse biases. As shown in Fig. 10(c), corresponding carrier transport is displayed. Due to the difference of Fermi levels of NiO and Ga_2O_3, the Ga_2O_3/NiO heterojunction was in a non-thermal equilibrium state. When they contacted, the electron would flow from Ga_2O_3 to NiO, until the Fermi levels were even up. Meanwhile, a space charge region was developed across the interface of Ga_2O_3/NiO heterojunction, the built-in electric field ($E_{\text{built-in}}$) that is a key factor influencing device performances,[110] which is a basis for self-powered operation. Besides, the Pt nanoparticles may well form a localized field with Ga_2O_3, that could enhance the carrier transport and injection.[99]

Furthermore, an organic-inorganic hybrid heterojunction highlights simple and cost-effective synthesis methods, precise control of materials properties at different scales, and adjustable structure–performance relationships.[111] Ga_2O_3-based organic-inorganic hybrid heterojunction photodetectors have also received attention in solar-blind UV wavebands. As shown in Fig. 10(d), it is a schematic diagram of a Ga_2O_3/PEDOT:PSS heterojunction photodetector. To maximize the interaction between light and Ga_2O_3 (and PEDOT:PSS), the LSPR caused by Pt nanoparticles was introduced at the interface of Ga_2O_3/PEDOT:PSS heterojunction, instead of surface modification as shown in Figs. 10(a)–10(c). This kind of interface modification may cause resonance coupling at either side of the Ga_2O_3/PEDOT:PSS heterojunction. As observed in Fig. 10(e), after Pt nanoparticle decoration at the interface, the photo response performance has been improved. The I_{photo} increased and the I_{dark} decreased. According to the absorption spectra in Fig. 10(f), the prepared Pt nanoparticles had strong absorbance and LSPR coupling in the solar-blind UV region. A larger Pt nanoparticle had higher light absorbance. In Fig. 10(g), a near-field enhancement effect is observed by Pt nanoparticle LSPR coupling with increasing sizes (from 20 nm to 40 nm). The incident light could be coupled by Pt nanoparticles and pass through the cross section of Pt nanoparticles as electromagnetic waves. Then, the

light absorption was significantly improved in the active region. As shown in Fig. 10(h), the spectral response is given. The photo response of Pt-decorated photodetector had higher R, since massive hot electrons were excited and injected into the conduction band of Ga_2O_3, which can contribute to higher I_{photo}, as shown in Fig. 10(i).

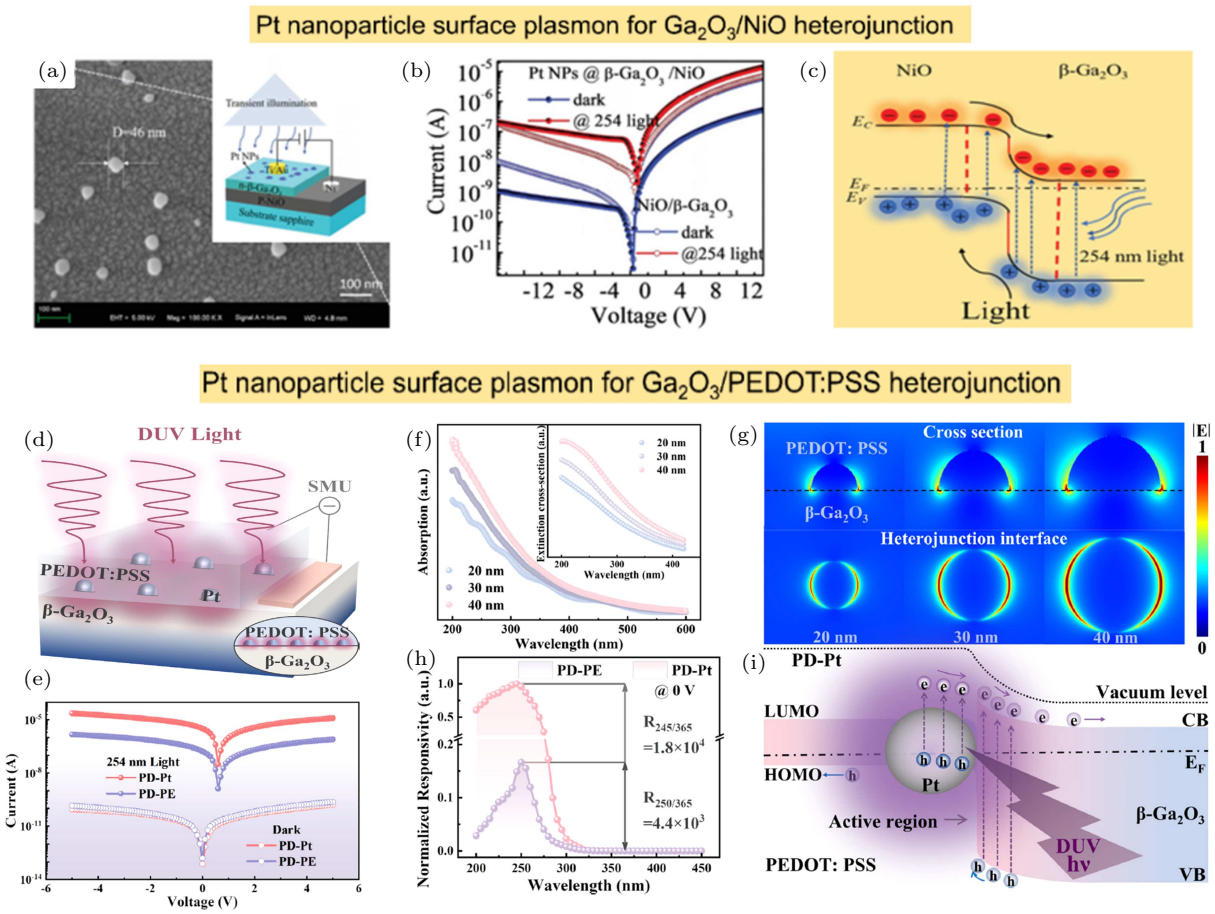


Fig. 10. Pt nanoparticles surface plasmons enhanced Ga_2O_3/NiO heterojunction photodetector: (a) SEM image of the Pt nanoparticles on Ga_2O_3 thin film, inset is the schematic of Ga_2O_3/NiO heterojunction photodetector, (b) the current–voltage curves of Pt nanoparticles decorated heterojunction photodetector in the dark and under illuminations, and (c) its energy-band diagram under 254 nm light illumination, reproduced with permission from Ref. [109], Copyright 2020, IEEE. Pt nanoparticles surface plasmons enhanced Ga_2O_3/PEDOT:PSS heterojunction photodetector: (d) the schematic diagram and enhanced mechanism, (e) current–voltage curves in the dark and under illuminations for the photodetectors with and without Pt nanoparticles decoration, (f) absorbance and extinction characteristics, (g) the cross-section electric field distribution of the heterojunction decorated by Pt nanoparticles, (h) spectral response, (i) carrier transport in energy-band diagram, reproduced with permission from Ref. [112], Copyright 2024, IEEE.

4. Complex metal nanoparticles

In addition to the nanoparticles and nanospheres made of single metal. The plasmons could also have different components and more complex structures, translating to many desired properties.[70] Beyond discussing the plasmon enhancement in photoconductive detectors, the effects of Ga–In nanoparticle plasmons on Ga_2O_3-based heterojunction photodetection was also induced as shown in Fig. 11.[113] Figure 11(a) is the schematic diagram of the Ga–In nanoparticle plasmons enhanced Ga_2O_3/CuO heterojunction photodetector. The cross-section FE-SEM image of the heterojunction is shown in Fig. 11(b), the thicknesses of Ga_2O_3 and CuO were 117 nm and 115 nm, respectively. The morphology of the Ga–In nanoparticles is displayed in Fig. 11(c), and inset is the absorbance spectrum. Its photo response peak located at the solar-blind UV region, showing the coupling ability with Ga_2O_3. As shown in Fig. 11(d), the Ga–In nanoparticles enhanced Ga_2O_3/CuO heterojunction photodetector could response to 254 nm, 302 nm and 365 nm UV light. Under 254 nm light illumination, the highest I_{photo} was obtained. Figure 11(e) is the schematic for explaining the LSPR enhancement mechanism for this Ga_2O_3/CuO heterojunction photodetector. The electrons at the surface of Ga–In metal would oscillate collectively be excited by incident UV light, i.e., plasmon resonance. It occurs when the frequency of the incident light resonates with the oscillation of electrons. Meanwhile, the incident electromagnetic wave decreased with the depth of Ga–In metal. So, the resonance always happens at the surface of metal. The introduced Ga–In nanoparticles enhanced the localized electric field, up to several orders of magnitude near the surface of the Ga–In nanoparticles. The total output I_{photo} include the conduction electrons in active Ga_2O_3 layer and the excited hot electrons by LSPR under illuminations.

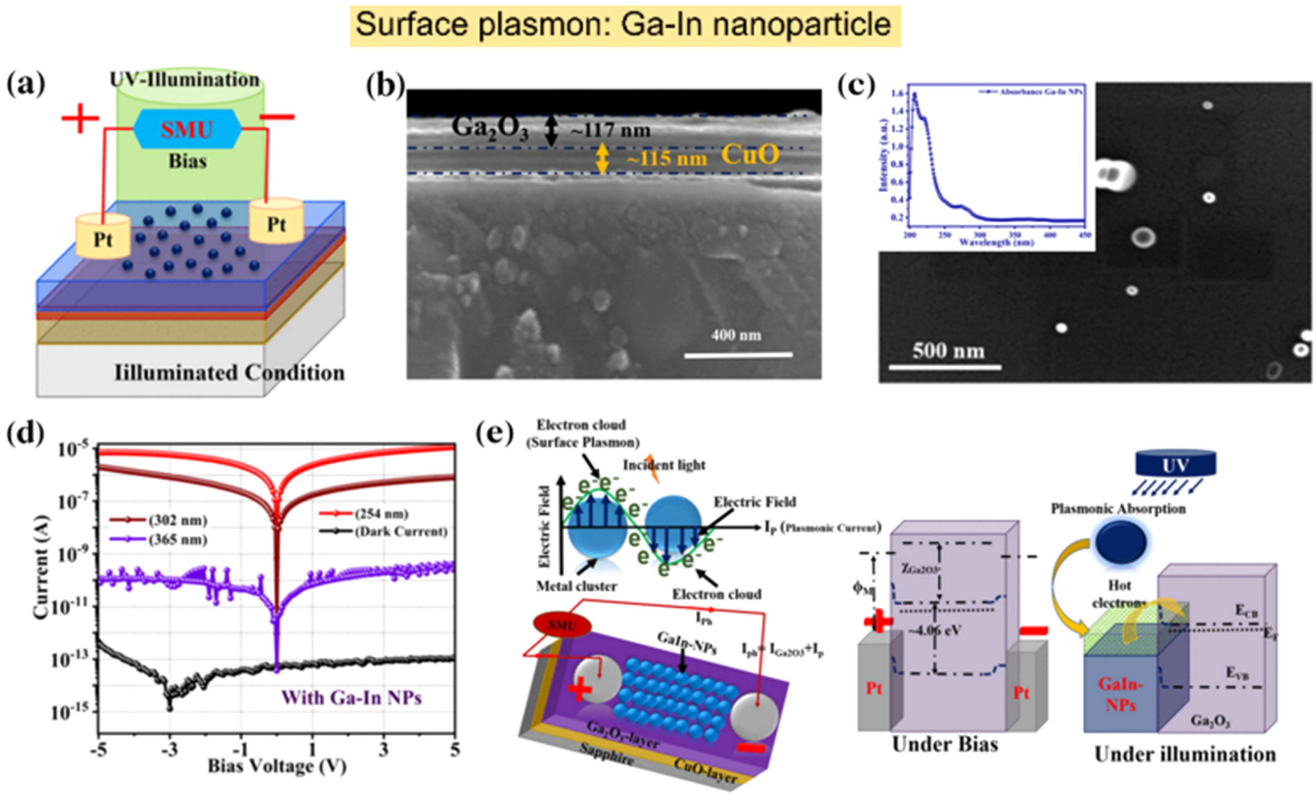


Fig. 11. Ga–In nanoparticles surface plasmons enhanced Ga_2O_3-based photodetector on CuO: (a) schematic of Ga_2O_3 photodetector on CuO, (b) cross-section SEM image of the Ga_2O_3/CuO heterojunction, (c) SEM image of the Ga–In nanoparticles, (d) current–voltage curves in the dark and under illuminations (254 nm, 302 nm and 365 nm), (e) energy-band diagram of the Ga_2O_3-based photodetector on CuO that is decorated by Ga–In nanoparticles, reproduced with permission from Ref. [113], Copyright 2022, IEEE.

Particularly, Qian *et al* .[114] reported an ultra-sensitive Ga_2O_3-based photodetector improved by Al@Al_2O_3 core–shell nanostructure arrays. The schematic diagram of the photodetector is shown in Fig. 12(a). Figure 12(b) is a top-view SEM image of the Ga_2O_3-based metal–semiconductor–metal photodetector with Al@Al_2O_3 nanostructure, whose detailed schematic diagram is in Fig. 12(c). This could extend the plasmonic properties into the solar-blind UV applications. This well-defined Al@Al_2O_3 core–shell nanostructure of sub-50 nm sizes features narrow dimension distribution, periodic patterns, and high densities. Its field-emission scanning electron microscope (FE-SEM) image is shown in Fig. 12(d). Al nanostructure arrays of different dimensions on the Ga_2O_3 thin film are displayed with only a few defects. Then, the hexagonal patterns were transferred to Al nanoparticles, which form a well-defined Al nanostructure array with a periodic graphene-like pattern. The diameter of the Al nanosphere changed with the dimensions of the Al nanostructure, with an average of 42 nm, 45 nm, and 48 nm, respectively. As shown in Fig. 12(e), from the absorbance spectra, the light absorbance was enhanced after Al@Al_2O_3 core–shell nanostructure decoration, compared to the pristine Ga_2O_3 thin film. Figure 12(f) illustrates the extinction spectra of the isolated Al@Al_2O_3 nanostructure of various dimensions. They all have peaks, indicating the existence of LSPR in these decorated photodetectors. From these spectra, we can see that the LSPR energy depends sensitively on the Al_2O_3 shell structure. The dipolar resonance red-shifts by $\sim$ 22 nm, and the extinction amplitudes are slightly decreased as well. This is due to the modified dielectric environment by surface oxide Al_2O_3.[115] This is because the enhanced phase delay can reduce the number of oscillating electrons and shift the plasmon frequency to red along with a shorter lifetime.[116,117] Moreover, a larger nanostructure dimension can induce further red-shift of the coupling wavelengths together with higher resonance amplitude. This is possibly due to the enlarged absorbance cross section. Starting from the fact that the Al was prepared on the Ga_2O_3 thin film, many localized Schottky junctions between Al and Ga_2O_3 were developed, i.e., Al/Ga_2O_3 junction as shown in Fig. 12(g). When UV light with matched resonance frequency is incident on the photodetector, the light would pass through the Al_2O_3 shell part and arrive at the Al core part, leading to the collective oscillation of free electrons. Thus, the localized electromagnetic field was enhanced. During this process, the plasmonic energy could be re-radiated through scattering, and the light absorbance for the active Ga_2O_3 thin film was improved. Besides, non-radiative plasmons could also release hot electrons that can inject into Ga_2O_3, overcoming localized Schottky barriers. Thus, a larger I_{photo} can be achieved by designing such a plasmonic structure.

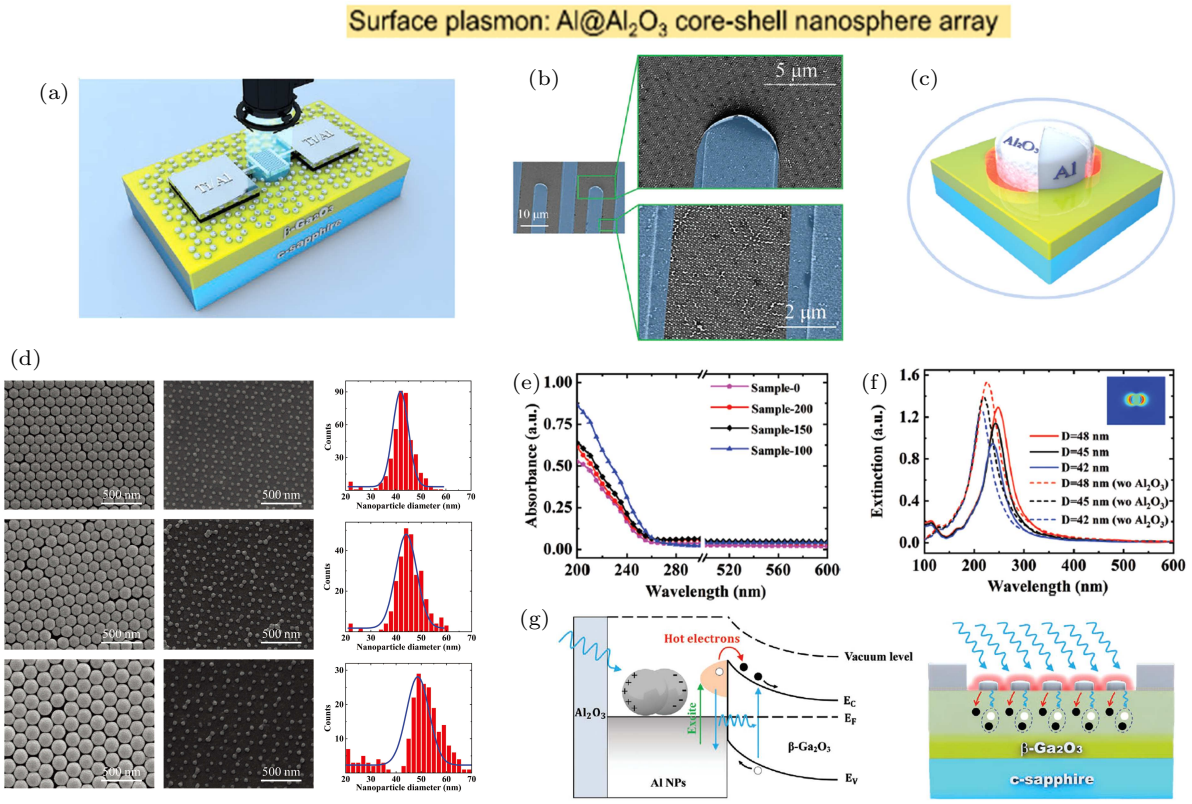


Fig. 12. Al@Al_2O_3 core–shell nanoparticles array enhanced Ga_2O_3-based photodetector: (a) schematic of the photodetector and (b) its top-view image, (c) schematic of Al@Al_2O_3 core–shell nanoparticles, (d) SEM images of the as-prepared and resulting Al nanoparticles, arrays and extracted Gaussian fitted dimensions, (e) absorbance spectra of the photodetectors with and without Al@Al_2O_3 core–shell nanoparticles array, (f) simulated extinction spectra of the Al@Al_2O_3 core–shell nanoparticles based on isolated model, (g) energy-band diagram and device in operation, reproduced with permission from Ref. [114], Copyright 2022, Wiley-VCH GmbH.

5. Bipolar broadband photodetection

According to the results in Fig. 10(d), LSPR-enhanced Ga_2O_3-based photodetector could perform broadband photodetection. Arora *et al.*[118] reported a highly sensitive and broadband photodetector based on Ag nanoparticle-decorated Ga_2O_3 thin film, sensing UV-A and UV-C wavebands. Importantly, this reported work breaks conventional unipolar photo-response, showing a polarity change of I_{photo} for different wavebands of irradiated light. Ag nanoparticles were deposited on the surface of Ga_2O_3 thin film, and the corresponding schematic diagram of the photodetector is shown in Fig. 13(a). The LSPR in these Ag nanoparticles contributed to an ultra-high R of 250 A/W until 2020, suggesting ultra-high photoelectronic conversion efficiency. The R was +157 μA/W under UV-C light and −353 μA/W under UV-A light, showing a bipolar photo-response characteristic.[119] The observed current reversal phenomenon can be owing to the charge carrier dynamics stemming from the hot electrons' generation. Figure 13(b) shows the UV-visible absorbance spectra of Ga_2O_3 photodetectors with and without Ag nanoparticle decoration. Obviously, the Ag nanoparticle-decorated Ga_2O_3 photodetector had an absorbance around 400 nm, and relatively broadband absorbance in the deep UV region of 200–280 nm. The absorbance was improved after introducing Ag nanoparticles. Compared to the bare Ga_2O_3 photodetector, the absorbance at 400 nm for the decorated photodetector is due to the existence of Ag nanoparticles. The hot electrons were excited and injected from Ag to Ga_2O_3. Figure 13(b) inset indicates the Ag nanoparticles could absorb UV-A light of 370 nm. Based on these, what can be concluded is that the introduction of Ag nanoparticles in Ga_2O_3 photodetector can increase the light absorbance in UV-A region and boost the Ga_2O_3 photodetector to operate at two bands. In addition, the absorbance peak had slightly shifted, since the dielectric environment varied. As seen from Fig. 13(c), the R of the Ga_2O_3 photodetector has increased from 88.02 A/W to 251.74 A/W with a 285% increase rate, after Ag nanoparticle surface modification at 5 V bias under illumination with an intensity of 44 nW/cm^2. Such a surface engineering had improved the ability to detect ultra-weak light signal. Besides, a R peak of 12.62 A/W at UV-A waveband certified the broadband photodetection. Overall, this photodetector had a photo-response in a broad waveband from 250 nm to 400 nm. In addition, as shown in Fig. 13(d), the mechanism for bipolar photodetector at UV-A and UV-C bands is illustrated by energy-band theory, in which the Au electrodes are used with a work function ($E_{F,Au}$) of ∼ 5.10 eV.[97] Since the electron affinity of Ga_2O_3 (χ_{GO}) is about 4.00 eV,[98] the equilibrium would be achieved by transferring electrons from Ga_2O_3 to Au. Once the Fermi levels are at the same level, the electrons at the Au side are more numer-

ous than those at the Ga_2O_3 side. Correspondingly, net positive charges were accumulated at the Ga_2O_3 side, translated to a potential barrier when Au and Ga_2O_3 were aligned. Hence, a Schottky barrier height was developed. Importantly, it is seriously influenced by the interfacial defects.[120,121] The interface modification can tune the barrier height at both metal–semiconductor interfaces, and then adjust the photodetection performances, especially at zero bias. After introducing Ag nanoparticles, whose work function is about 4.26 eV, higher than χ_{GO}, this would lead to the downward band bending of Ga_2O_3 to create a Schottky barrier. When UV-C (254 nm, 4.88 eV) light illuminated the photodetector, the Ag nanoparticles could not exhibit plasmon resonance. The electrons in the valence band would be excited to the conduction band, while the holes remained in the valence band. The electron–hole pairs separated at the metal–semiconductor interface, which can cause a change in the direction of I_{photo}. However, under UV-A light illumination, a reversal in the direction of I_{photo} was achieved. The introduced Ag nanoparticles chiefly absorb UV-A light since Ag nanoparticles have high absorbance in the UV-A waveband. Under UV-A light illumination, the electrons are excited to have high energy, higher than the conduction band of Ga_2O_3. Under such a condition, the irradiated and non-irradiated plasmons will cause hot electron injection into the active Ga_2O_3 layer in the photodetector. Because the photon energy of UV-A light is larger than the E_g of Ga_2O_3, the direct carrier generation from the valence band to the conduction band may be negligible. Therefore, the direction of I_{photo} was changed. So, a bipolar broadband Ga_2O_3-based photodetector decorated with Ag nanoparticle surface plasmons was developed. As a result, as displayed in Fig. 13(e), the positive I_{photo} was 5.43×10^{-10} A under UV-C light illumination, translating to a R of 0.157×10^{-4} A/W. Meanwhile, as shown in Fig. 13(f), the negative I_{photo} was -6.47×10^{-10} A under UV-C light illumination, and R was 3.53×10^{-4} A/W.

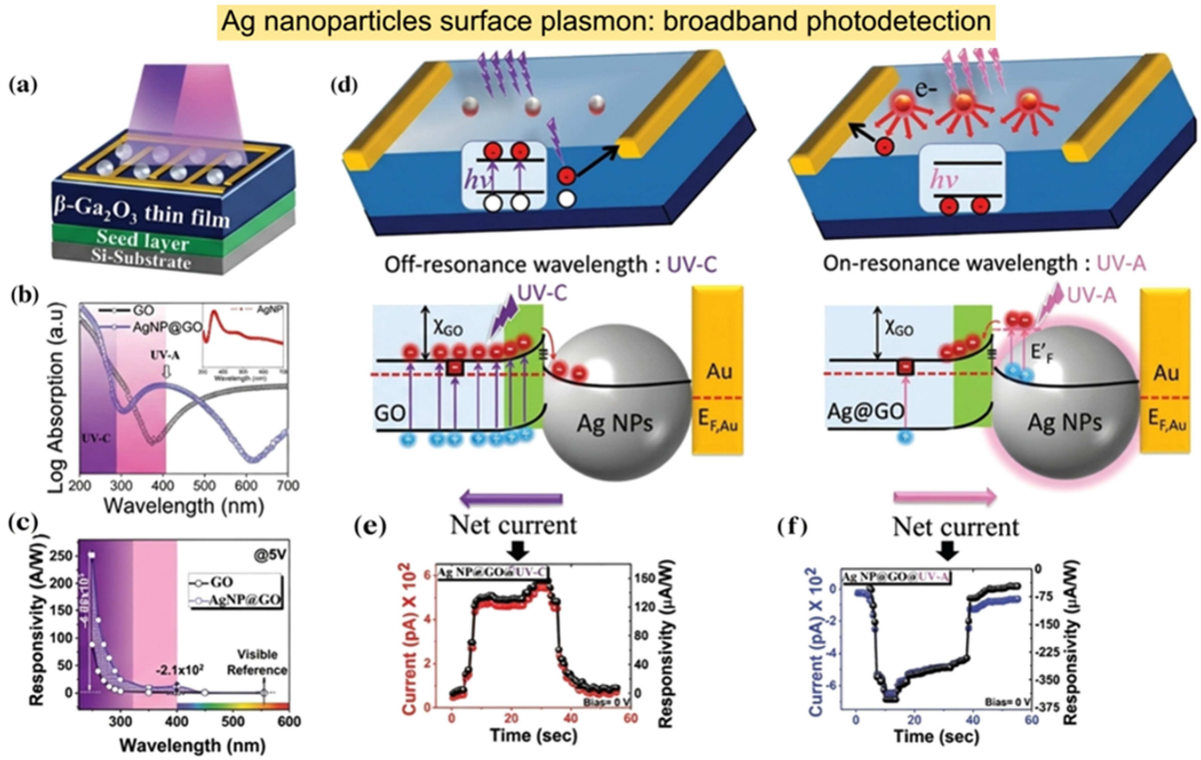


Fig. 13. Ag nanoparticles surfaces plasmons contribute to the enhanced performance and broadband photodetection of the Ga_2O_3-based photodetector: (a) schematic of photodetector, (b) absorbance spectra and (c) responsivity of photodetector with and without Ag nanoparticles, (d) schematic and energy-band diagrams of the photodetector under UV-A and UV-C light illuminations, response time under (e) UV-C and (f) UV-A light illuminations. Reproduced with permission from Ref. [118]. Copyright 2020, Wiley-VCH GmbH & Co. KGaAm Weinheim.

6. Subwavelength surface plasmon polariton (SPP) waveguides

The surface plasmon technique is a subwavelength optical method to merge photonics and electronics at the nanoscale.[46,47] As partly mentioned in Section 4, the structural design of surface nanostructures could provide more tunable degrees of freedom for achieving the development of nanophotonic devices.[122,123] Owing to the unique advantages of nanostructured metal to confine and enhance light absorption at the metal–semiconductor interface, designed surface plasmons have shown promise.[73,124] Wang *et al.* reported a Ru nanograting-enhanced Ga_2O_3 photodetector using LSPR.[125] Figure 14(a) is the schematic diagram of the nanograting-enhanced Ga_2O_3 photodetector. The SEM image of the Ru nanograting structure is displayed in Fig. 14(b),

with a periodic arrangement. In Fig. 14(c), the nanograting-enhanced Ga_2O_3 photodetector had a R of 13.02 mA/W, which was 490 times larger than that without the nanograting structure. In addition, the enhanced photodetector also had a high specific detectivity of 4.11×10^{10} Jones, suggesting highly sensitive photodetection ability. This Ru nanograting-enhanced Ga_2O_3 photodetector could generate plasmonic excitations to improve light absorption and photosensitivity. As shown in Fig. 14(d), the nanograting-enhanced Ga_2O_3 photodetector had rise and decay times of 0.96 s and 0.14 s, respectively. They are much shorter than those of 1.57 s and 0.47 s for the non-decorated Ga_2O_3 photodetector. This is owing to the increase in carrier separation efficiency caused by the Ru nanograting LSPR. To understand the mechanism of this enhanced photodetector, its energy-band diagram is shown in Figs. 14(e)–14(g). In Fig. 14(e), the dipole moments are developed at the interface of Ru and Ga_2O_3 when irradiated by incident light. This would lead to the coupling and scattering of the incident photons. It can prolong the light paths and enhance the light absorption efficiency of the Ru nanograting LSPR-enhanced Ga_2O_3 photodetector. Figure 14(f) indicates the electromagnetic field across the Ru nanograting structure. When the Ru nanograting structure is irradiated by incident UV light, LSPR enhancement is induced in the detector, generating electron–hole pairs and increasing its effective absorption cross-section. The LSPR effect concentrates the incident light in the vicinity of the Ru nanograting to improve the light-trapping efficiency. Therefore, the strongly localized electric field in the vicinity of the Ru nanograting coupled with the increased optical paths of incident photons can improve light absorption ability, thereby contributing to more electron–hole pair generation. Subsequently, an increased number of electrons are transferred from the Ru metal to the conduction band of the Ga_2O_3 semiconductor, as shown in Fig. 14(g). This enhancement promotes their migration into the Ga_2O_3 films, facilitating the generation and separation of photogenerated carriers. Increased electron transfer leads to a higher output current, ultimately improving the optoelectronic performance of the devices.

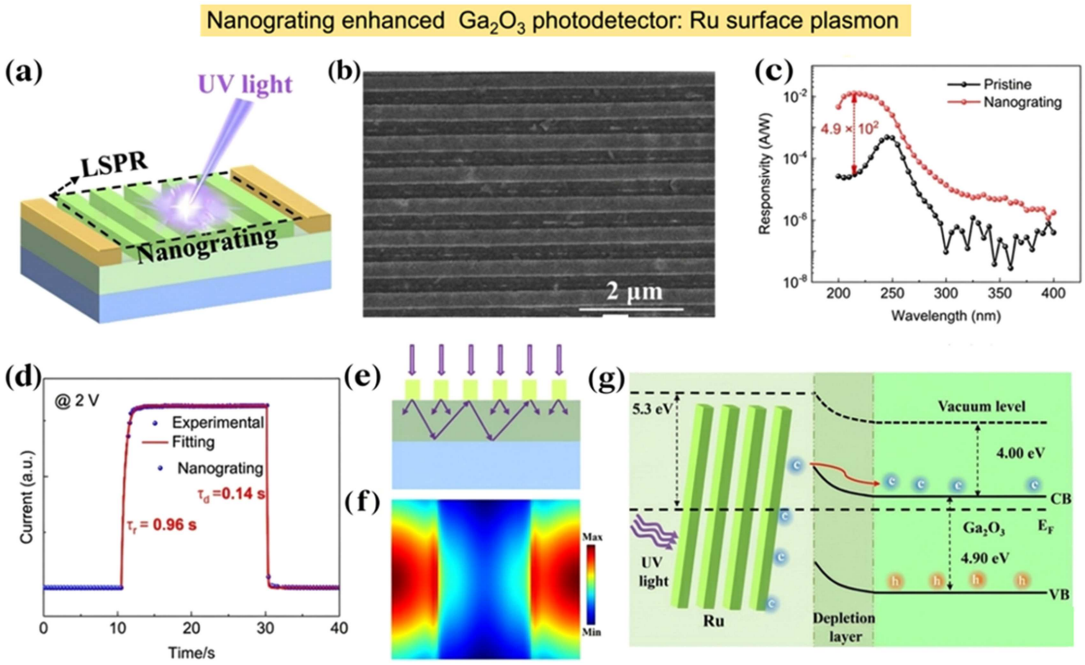


Fig. 14. Ru nanograting structure enhanced Ga_2O_3-based photodetector: (a) schematic of photodetector, (b) SEM image of Ru nanograting structure, (c) responsivity of photodetectors with and without Ru nanograting structure, (d) response time of photodetector with nanograting structure, (e) light trapping in the nanograting structure, (f) simulated electric field at y–x cross-section across the interface of Ru nanograting and Ga_2O_3 thin film, (g) schematic energy-band diagram of Ru nanograting enhanced photodetector. Reproduced with permission from Ref. [125], Copyright 2025, American Chemical Society.

7. Summary

In summary, the photodetection performances are improved via introducing metal nanoparticles surface plasmons, through hot electrons excitation and injections, and LSPR. To some extent, it overcomes the limitation of light diffraction for manipulating light. The enhanced performance achieved in Ga_2O_3-based photoconductive detectors, photodetector array, heterojunction photodetectors are fully reviewed and discussed. In addition, the design of metal nanostructure, the development of broadband photodetection, bipolar transports, and subwavelength nanograting optics are further discussed for enhancing Ga_2O_3-based photodetectors.

The working mechanism for hot electron transfer and LSPR is illustrated for understanding the recent progress. For the interaction between incident photons and electrons in Ga_2O_3, the hot electrons, excited and escaping outside the

metal, could transfer and inject into the photoactive layer and contribute to the I_{photo}. When the optical E_g is close to the excitation energy for the used metal, the strong coupling resonance increases the light absorbance of the decorated photodetectors. The metal nanostructure, a type of surface plasmons, plays a key role in confining light and enhancing the localized electromagnetic field. At the nanoscale dimension, the electrons in the conduction band could undergo collective oscillation, which has developed into a pathway for investigating surface and interface phenomena in nanoscale photonics and optoelectronics.

Tuning the metal nanostructure could change the resonance frequency, thus affect the interaction between light and Ga_2O_3. In which, the metal nanostructures decorated surface and interface become an important issue for Ga_2O_3-based optoelectronics, remain a nontrivial and open challenge. Especially, the small nanoparticles could decrease the scattering intensity owing to the tiny scattering cross sections. Besides, for small sized metal nanoparticles, the light absorbance can be improved via amplifying the surface electric field, rather than changing the sizes and shapes. A good design of metal nanostructures controlling intrinsic losses is till on-demand.

Surrounding dielectric environmental interference is also an obstacle for Ga_2O_3 to be practical. It may cause a large intrinsic dissipation of LSPR, seriously hindering the actual applications. However, less attention is paid to Ga_2O_3-based photodetection devices. This topic could involve further study on the plasmon mode and complex interfaces.

The surface-plasmon-enhanced Ga_2O_3-based photodetectors contribute to high optical gain, pushing them to be applied in quantum optics, surface enhanced Raman scattering (SERS), optoelectronic multiple tube, nanoscale laser, etc.

Despite the significant progress achieved in plasmon-enhanced Ga_2O_3 photodetectors, several challenges and opportunities remain for future research. First, precise control over the size, morphology, and spatial distribution of metal nanostructures is essential to achieve tunable and reproducible plasmonic responses. Advanced nanofabrication techniques and self-assembly strategies may provide effective solutions. Second, the trade-off between enhanced photoresponsivity and increased dark current induced by metal integration needs to be carefully optimized, particularly through interface engineering and dielectric interlayers. Third, further exploration of novel plasmonic materials, such as transition metal nitrides and two-dimensional materials, may offer improved thermal stability and compatibility with semiconductor processing. Additionally, coupling plasmonic effects with emerging mechanisms, such as pyro-phototropic and piezo-phototropic effects, could open new pathways for multifunctional photodetection. Finally, the integration of Ga_2O_3 plasmonic photodetectors into array systems and on-chip platforms remains a key step toward practical applications in imaging, optical communication, and environmental monitoring.

In terms of practical applications, plasmon-enhanced Ga_2O_3 photodetectors show strong potential in solar-blind UV imaging, missile warning systems, environmental monitoring, flame detection, and secure optical communications. Their capability for high sensitivity and fast response also makes them promising candidates for integrated photonic circuits and next-generation wearable optoelectronic systems.

Acknowledgements

This work was supported by the National Natural Science Foundation of China (Grant Nos. 62564011, 62204125, U23A20349, and 62501320), the Steed Plan of Inner Mongolia University for Introducing High-Level Talents (Grant Nos. 10000-A24199006 and 10000-A24106015), the Inner Mongolia University Experimental Technology Research Project in 2026 (Self-Made and Modified Equipment Project) (Grant No. SYJS2026007), the Inner Mongolia Autonomous Region-level Scientific Research Startup Fund (Grant Nos. 21700-252904 and 21700-252905), the Program for Innovative Research Team in Universities of Inner Mongolia Autonomous Region of China (Grant No. NMGIRT2503), the Basic Scientific Research Funding for Universities Directly Affiliated with the Inner Mongolia Autonomous Region of China (Grant No. 2026JBKY002), and the Young Scientists Fund (Type A) of the Natural Science Foundation of Inner Mongolia Autonomous Region of China (Grant No. 2026QA016).

References

[1] Shockley W and Pearson G L 1948 *Phys. Rev.* **74** 232
[2] Zhu J, Cai Q, Shao P, Zhang S, You H, Guo H, Wang J, Xue J, Liu B, Lu H, Zheng Y, Zhang R and Chen D 2025 *Nat. Commun.* **16** 1186
[3] Wang H, Zhou C, Li P, Yang L, Ma J, Akaike R, Miyake H, Xu H and Liu Y 2025 *Nat. Commun.* **16** 8175
[4] Liu Z, Xi Z, Gu L, Yan S, Zhang R, Zhang X, Wang H, Zhang J H and Tang W 2025 *Nanotechnology* **36** 362001
[5] Liu Z, Xi Z, Gu L, Yan S, Li L, Shu L, Zhang J, Zhang S, Bian A, Jiang M and Tang W 2025 *Laser Photon. Rev.* **19** e01855
[6] Nguyen T M H, Shin S G, Choi H W and Bark C W 2022 *Exploration* **2** 20210078
[7] Diffey B L 2002 *Methods* **28** 4
[8] Chen X, Ren F, Gu S and Ye J 2019 *Photon. Res.* **7** 381
[9] Cao F, Liu Y, Liu M, Han Z, Xu X, Fan Q and Sun B 2024 *Research* **7** 0385
[10] Li T, Emon M J H, Rahad R, Chatterjee A, Dalakoti V, Liu J, Yu H, Mi Z, Huang S and Zhao Y 2025 *Opt. Mater. Express* **15** 2383
[11] Liu N, Fang G, Zeng W, Zhou H, Cheng F, Zheng Q, Yuan L, Zou X and Zhao X 2010 *ACS Appl. Mater. Interfaces* **2** 1973
[12] Ouyang B, Zhang K and Yang Y 2018 *iScience* **1** 16
[13] Ouyang W, Chen J, Shi Z and Fang X 2021 *Appl. Phys. Rev.* **8** 031315
[14] Ji Y, Li G, Liu H, Zhang S T, Wang W, Li D and Cui Y 2024 *J. Phys. D: Appl. Phys.* **58** 025108
[15] Sha S, Tang K, Liu M, Wan P, Liu Z, Shi D N, Kan C and Jiang M 2024 *ACS Photon.* **11** 4472
[16] Huang C, Zhang H and Sun H 2020 *Nano Energy* **77** 105149
[17] Xie Z, Jiang K, Zhang S, Wang Z, Shan X, Wang B, Ben J, Liu M, Lv S, Chen Y, Jia Y, Sun X and Li D 2025 *Adv. Mater.* **37** 2419316
[18] Song W, Chen J, Li Z and Fang X 2021 *Adv. Mater.* 33 e2101059

[19] Li K H, Fu W Y, Cheung Y F, Wong K K Y, Wang Y, Lau K M and Choi H W 2018 *Optica* **5** 564
[20] Jia L, Zhu S, Zhang N, Lin Z, Cai W, Cheng L, Lu X and Zheng W 2025 *Adv. Opt. Mater.* **13** 2402601
[21] Zhang D, Cheng L, Song X, Zhang X, Zhang L, Zhu S, Hu M, Liu Y, Ouyang X and Zheng W 2025 *Angew. Chem. Int. Ed.* **64** 202505665
[22] Lin Z, Zhu S, Wang Z, Jia L, Zhang N, Zhang C and Zheng W 2025 *Mater. Today* **86** 202
[23] Li Z, Yan T and Fang X 2023 *Nat. Rev. Mater.* **8** 587
[24] Yang J, Liu K, Chen X and Shen D 2022 *Prog. Quantum Electron.* **83** 100397
[25] Chen H, Liu K, Hu L, Al-Ghamdi A A and Fang X 2015 *Mater. Today* **18** 493
[26] Tian K, Pei Z, Feng S, Chu C, Huang F, Zhang Y, Sun X W and Zhang Z H 2025 *Opt. Express* **33** 10609
[27] Yu H, Memon M H, Wang R, Xiao S, Li D, Luo Y, Wang D, Gao Z, Yao J, Shen C, Li S, Zheng J, Zhang J, Ooi B S, Liu S and Sun H 2024 *Adv. Opt. Mater.* **12** 2400499
[28] He X, Sun R, Xu X, Geng H, Qi S, Zhang K H and Long H 2024 *ACS Appl. Mater. Interfaces* **16** 64146
[29] Varshney U, Aggarwal N and Gupta G 2022 *J. Mater. Chem. C* **10** 1573
[30] Xie X H, Zhang Z Z, Li B H, Wang S P, Jiang M M, Shan C X, Zhao D X, Chen H Y and Shen D Z 2013 *Appl. Phys. Lett.* **102** 231122
[31] Liang H L, Mei Z X, Zhang Q H, Gu L, Liang S, Hou Y N, Ye D Q, Gu C Z, Yu R C and Du X L 2011 *Appl. Phys. Lett.* **98** 221902
[32] Liu Z, Wang X, Liu Y, Guo D, Li S, Yan Z, Tan C K, Li W, Li P and Tang W 2019 *J. Mater. Chem. C* **7** 13920
[33] Liu Z, Li P G, Zhi Y S, Wang X L, Chu X L and Tang W H 2019 *Chin. Phys. B* **28** 017105
[34] Liu Z and Tang W 2023 *J. Phys. D: Appl. Phys.* **56** 093002
[35] Wu G, Guo X, Zhu Z, Song H, Zhong X, Wang J and Guo D 2025 *IEEE Trans. Electron Devices* **72** 6814
[36] Wu G, Guo X, Zhang F, Zhong X, Wang J and Guo D 2025 *IEEE Electron Device Lett.* **46** 2086
[37] Pan J, Li C, Geng H, Ni Y, Wu C, Wu H, Wang S, Wu F and Guo D 2025 *Phys. Rev. Appl.* **24** 064043
[38] Pearton S J, Yang J, Cary P H, Ren F, Kim J, Tadjer M J and Mastro M A 2018 *Appl. Phys. Rev.* **5** 011301
[39] Kaur D and Kumar M 2021 *Adv. Opt. Mater.* **9** 2002160
[40] Oshima T, Okuno T and Fujita S 2007 *Jpn. J. Appl. Phys.* **46** 7217
[41] Oshima T, Okuno T, Arai N, Suzuki N, Ohira S and Fujita S 2008 *Appl. Phys. Express* **1** 011202
[42] Zeng Y, Huang H, Zhao X, Ding M, Hou X, Zou Y, Du J, Liu J, Yu S, Han K, Wu Y, Zhou X, Xu G and Long S 2023 *IEEE Electron Device Lett.* **44** 2003
[43] Pearton S J, Ren F, Polyakov A Y, Haque A, Labed M and Rim Y S 2025 *Appl. Phys. Rev.* **12** 031336
[44] Pendry J 1999 *Science* **285** 1687
[45] Xu D, Xiong X, Wu L, Ren X F, Png C E, Guo G C, Gong Q and Xiao Y F 2018 *Adv. Opt. Photon.* **10** 703
[46] Ozbay E 2006 *Science* **311** 189
[47] Barnes W L, Dereux A and Ebbesen T W 2003 *Nature* **424** 824
[48] Tan S, Argondizzo A, Ren J, Liu L, Zhao J and Petek H 2017 *Nat. Photon.* **11** 806
[49] Einstein A 1905 *Ann. Phys.* **322** 132
[50] Schaadt D, Feng B and Yu E T 2005 *Appl. Phys. Lett.* **86** 063106
[51] Li D, Sun X, Song H, Li Z, Chen Y, Jiang H and Miao G 2012 *Adv. Mater.* **24** 845
[52] Mani M, Mariandry K, Ghorpade U V, Saha S, Kokate R, Mishra R, Nielsen M P, Tilley R, Xie B, Suryawanshi M P and Kumar P V 2025 *Small* **21** 2410173
[53] Liu N, Wei H, Li J, Wang Z, Tian X, Pan A and Xu H 2013 *Sci. Rep.* **3** 1967
[54] Dan Y, Zhao X, Chen K and Mesli A 2018 *ACS Photonics* **5** 4111
[55] Gramotnev D K and Bozhevolnyi S I 2010 *Nat. Photonics* **4** 83
[56] Homola J 2018 *Chem. Rev.* **108** 462
[57] Anker J N, Hall W P, Lyandres O, Shah N C, Zhao J and Van Duyne R P 2008 *Nat. Mater.* **7** 442
[58] Huang Y, Fang Y, Zhang Z, Zhu L and Sun M 2014 *Light: Sci. Appl.* **3** e199
[59] Russell K J, Liu T L, Cui S and Hu E L 2012 *Nat. Photonics* **6** 459
[60] Oulton R F, Sorger V J, Zentgraf T, Ma R M, Gladden C, Dai L, Bartal G and Zhang X 2009 *Nature* **461** 629
[61] Xu H X 2003 *Phys. Lett. A* **312** 411
[62] Xu H and Kall M 2002 *Phys. Rev. Lett.* **89** 246802
[63] Zayats A V, Smolyaninov I I and Maradudin A A 2005 *Phys. Rep.* **408** 131
[64] Kelly K L, Coronado E, Zhao L L and Schatz G C 2003 *J. Phys. Chem. B* **107** 668
[65] Bohren C F and Huffman D R 1998 *Absorption and Scattering of Light by Small Particles* (Wiley-VCH)
[66] Wan P, Jiang M, Tang K, Zhou X and Kan C 2020 *CrystEngComm* **22** 4393
[67] Wei H, Yan X, Niu Y, Li Q, Jia Z and Xu H 2021 *Adv. Funct. Mater.* **31** 2100889
[68] Hutter E and Fendler J H 2004 *Adv. Mater.* **16** 1685
[69] Lee K C, Lin S J, Lin C H, Tsai C S and Lu Y J 2008 *Surf. Coat. Technol.* **202** 5339
[70] Tian X, Tong L and Xu H 2013 *Sci. China Phys. Mech. Astron.* **56** 2327
[71] Wei H, Zhang S, Tian X and Xu H 2013 *Proc. Natl. Acad. Sci. USA* **110** 4494
[72] Zhu Y, Wei H, Yang P F and Xu H X 2012 *Chin. Phys. Lett.* **29** 077302
[73] Lan S, Rodrigues S P, Taghinejad M and Cai W 2017 *Laser Photon. Rev.* **11** 1600312
[74] Li Z, Zhang S, Tong L, Wang P, Dong B and Xu H 2014 *ACS Nano* **8** 701
[75] Hsieh C H, Chou L J, Lin G R, Bando Y and Golberg D 2008 *Nano Lett.* **8** 3081
[76] Wu Y J, Chen P H, Li J Y, Chou L J and Chen L J 2010 *ACS Nano* **4** 1393
[77] Xu H 2005 *Phys. Rev. B* **72** 073405
[78] Ritchie R H 1957 *Phys. Rev.* **106** 874
[79] An Y, Chu X, Huang Y, Zhi Y, Guo D, Li P, Wu Z and Tang W 2016 *Prog. Nat. Sci.: Mater. Inter.* **26** 65
[80] Qiao G, Cai Q, Ma T, Wang J, Chen X, Xu Y, Shao Z, Ye J and Chen D 2019 *ACS Appl. Mater. Interfaces* **11** 40283
[81] Shu L, Sha S, Zhang J H, Zhang S, Wang J, Ji X, Li S, Jiang M and Tang W 2024 *ACS Appl. Mater. Interfaces* **16** 54178
[82] Liu Z, Yu J, Li P, Wang X, Zhi Y, Chu X, Wang X, Li H, Wu Z and Tang W 2019 *J. Phys. D: Appl. Phys.* **52** 295104
[83] Shu L C, Sha S L, Yan S H, Li S, Ji X Q, Zhang J H, Jiang M M and Tang W H 2024 *IEEE Trans. Electron Devices* **71** 7747
[84] Cui S J, Mei Z X, Hou Y N, Chen Q S, Liang H L, Zhang Y H, Huo W X and Du X L 2018 *Chin. Phys. B* **27** 067301
[85] Cui S, Mei Z, Hou Y, Sun M, Chen Q, Liang H, Zhang Y, Bai X and Du X 2018 *Sci. China Phys. Mech. Astron.* **61** 107021
[86] Lin C, Wan P, Yang B, Shi D, Kan C and Jiang M 2023 *J. Mater. Chem. C* **11** 12968
[87] Sun Y, Jiang M, Li B, Xie X, Shan C and Shen D 2022 *Opt. Express* **30** 740
[88] Zhou X, Jiang M, Wu Y, Ma K, Liu Y, Wan P, Kan C and Shi D 2020 *Nanoscale Adv.* **2** 1340
[89] Terekhin P N, Benhayoun O, Weber S T, Ivanov D S, Garcia M E and Rethfeld B 2020 *Appl. Surf. Sci.* **512** 144420
[90] Losurdo M, Yi C, Suvorova A, Rubanov S, Kim T and Giangregorio M M, Jiao W, Bergmair I, Bruno G and Brown A S 2014 *ACS Nano* **8** 3031
[91] Cushing S K, Li J, Bright J, Yost B T, Zheng P, Bristow A D and Wu N 2015 *J. Phys. Chem. C* **119** 16239
[92] Li J, Cushing S K, Bright J, Meng F, Senty T R, Zheng P, Bristow A D and Wu N 2013 *ACS Catal.* **3** 47
[93] Zheng Z, Lu Y, Zhuang J, Jia L, Zhu S, Chen D, Qi H, Li T, Zhang H and Lu X 2025 *IEEE Electron Device Lett.* **46** 143
[94] Moore A, Rafique S, Llewelyn C, Lamb D and Li L 2025 *Adv. Electron. Mater.* **11** 2400898
[95] Tang R, Li G, Li C, Li J, Zhang Y, Huang K, Ye J, Li C, Kang J, Zhang R, Zheng Y and Zhang R 2020 *Opt. Express* **28** 5731
[96] Taguchi A, Saito Y, Watanabe K, Yijian S and Kawata S 2012 *Appl. Phys. Lett.* **101** 081110
[97] Michaelson H B 1977 *J. Appl. Phys.* **48** 4729
[98] Mohamed M, Irmscher K, Janowitz C, Galazka Z, Manzke R and Fornari R 2012 *Appl. Phys. Lett.* **101** 132106
[99] Wang X, Liu K, Chen X, Li B, Jiang M, Zhang Z, Zhao H and Shen D 2017 *ACS Appl. Mater. Interfaces* **9** 5574

[100] Yu J, Lou J, Wang Z, Ji S, Chen J, Yu M, Peng B, Hu Y, Yuan L, Zhang Y and Jia R 2021 *J. Alloys Compd.* **872** 159508

[101] Liu Z, Sha S L, Shen G H, Jiang M M, Zhang M L, Guo Y F and Tang W H 2023 *IEEE Electron Device Lett.* **44** 1324

[102] Shu L, Sha S, Xi Z, Li L, Yao S, Zhang J, Ji X, Zhang S, Bian A, Jiang M, Guo Y and Tang W 2024 *Sci. China Tech. Sci.* **67** 2449

[103] Zhi Y S, Liu Z, Zhang S H, Li S, Yan Z Y, Li P G and Tang W H 2021 *IEEE Trans. Electron Devices* **68** 3435

[104] Shen G H, Liu Z, Zhang M L, Guo Y F and Tang W H 2023 *IEEE Electron Device Lett.* **44** 1140

[105] Shen G, Liu Z, Tan C K, Jiang M, Li S, Guo Y and Tang W 2023 *Appl. Phys. Lett.* **123** 041103

[106] Kroemer H 2001 *Rev. Mod. Phys.* **73** 783

[107] Kroemer H 1983 *Surf. Sci.* **132** 543

[108] Kroemer H 1963 *Proc. IEEE* **51** 1782

[109] Yu J, Yu M, Wang Z, Yuan L, Huang Y, Zhang L, Zhang Y and Jia R 2020 *IEEE Trans. Electron Devices* **67** 3199

[110] Zhang J H, Li Z, Shen B, Liu Z, Chen L, Wang H, Li H, Zhang Y, Du S, Tang Q, Liu X, Li S, Du J, Yan K, Li Y, Hao X, Shi Y and Pan L 2024 *Cell Rep. Phys. Sci.* **5** 102025

[111] Zhou K, Qi B, Liu Z, Wang X, Sun Y and Zhang L 2024 *Adv. Funct. Mater.* **34** 2411671

[112] Zheng Z, Xiong Z, Xu L, Wu F, Kim M, Mao J, He Y, Xu J, Dai J and Chen C 2024 *IEEE Electron Device Lett.* **45** 633

[113] Kumar A, Ahuja J, Mondal A and Bag A 2022 *IEEE Trans. Nanotechnol.* **21** 196

[114] Qian L X, Li W, Gu Z, Tian J, Huang X, Lai P T and Zhang W 2022 *Adv. Opt. Mater.* **10** 2102055

[115] Zhang J H, Li Z, Liu Z, Li M, Guo J, Du J, Cai C, Zhang S, Sun N, Li Y, Xu X, Hao X and Yamauchi Y 2025 *Adv. Mater.* **37** 2419081

[116] Shimanoe K, Endo S, Matsuyama T, Wada K and Okamoto K 2021 *Sci. Rep.* **11** 5169

[117] Ekinci Y, Solak H H and Löffler J F 2008 *J. Appl. Phys.* **104** 083107

[118] Arora K, Singh D P, Fischer P and Kumar M 2020 *Adv. Opt. Mater.* **8** 2000212

[119] Wu G, Xu Y, Weng Y, Wu F and Guo D 2026 *Appl. Phys. Lett.* **128** 113305

[120] Lu M Y, Lu M P, You S J, Chen C W and Wang Y J 2015 *Sci. Rep.* **5** 15123

[121] Chiquito A J, Amorim C A, Berengue O M, Araujo L S, Bernardo E P and Leite E R 2012 *J. Phys. Condens. Matter* **24** 225303

[122] Koenderink A F, Alù A and Polman A 2015 *Science* **348** 516

[123] Maier S A, Kik P G, Atwater H A, Meltzer S, Harel E, Koel B E and Requicha A A 2003 *Nat. Mater.* **2** 229

[124] Wang J, Chen Z, Ji X, Liu Z, Zheng H, Liu Y, Li S, Tang W and Li P 2025 *Adv. Opt. Mater.* **13** e02309

[125] Wang J, Yang Y, Chen Z, Liu Z, Ji X, Yue J, Yan J, Li S, Tang W and Li P 2025 *ACS Appl. Nano Mater.* **8** 1277